Received: 3 July 2023 | Revised: 14 February 2024 | Accepted: 22 February 2024

DOI: 10.1002/qj.4726

Quarterly Journal of the Royal Meteorological Society RMetS

RESEARCH ARTICLE

Role of Bay of Bengal low-pressure systems in the formation of mid-tropospheric cyclones over the Arabian Sea and western India

Pradeep Kushwaha[1,2] | **Jai Sukhatme**[1,2] | **Ravi S Nanjundiah**[1,2]

[1]Center for Atmosphere & Ocean Sciences, Indian Institute of Science, Bangalore, India

[2]Divecha Centre for Climate Change, Indian Institute of Science, Bangalore, India

Correspondence
Pradeep Kushwaha, Centre for Atmospheric and Oceanic Sciences, Indian Institute of Science, Bangalore 560012, India.
Email: pkushwaha9999@gmail.com

Abstract

Arabian Sea mid-tropospheric cyclones (MTCs), responsible for extreme rainfall events in Western India, often coincide with monsoon low-pressure systems (LPSs) over the Bay of Bengal. However, the influence of Bay of Bengal LPSs on the formation of Arabian Sea MTCs remains unclear. This study utilizes the Weather Research and Forecasting Model (WRF) to investigate the atmospheric connection between these two basins. By introducing a balanced bogus vortex over the Bay of Bengal, cyclonic systems are induced over the Arabian Sea in the majority of ensemble members, exhibiting characteristics consistent with observations. In particular, as the Bay of Bengal vortex moves westward, the middle tropospheric trough deepens, horizontal wind shear increases, the low-level Arabian Sea stable inversion layer weakens, and the middle troposphere moisture content over Western India and the northeast Arabian Sea rises. Subsequently, MTC genesis occurs over the northeast Arabian Sea along the western edge of the trough within 2–4 days of model integration. A vorticity budget analysis highlights the critical role of vorticity advection and tilting during the initial 24 h of MTC genesis, while vortex stretching becomes the dominant vorticity source during rapid intensification. To substantiate these findings further, a mechanism denial experiment is conducted using a real-world instance of a coexistent Arabian Sea MTC and Bay of Bengal LPS, replicated in the model. In this experiment, conditions unfavorable for LPS genesis are created by cooling and drying the Bay of Bengal. The results demonstrate that the absence or reduced intensity of the Bay of Bengal LPS inhibits formation of the Arabian Sea MTC. In all, this study presents compelling evidence for the significant influence of Bay of Bengal low-pressure systems on the formation of severe weather-inducing MTCs over the Arabian Sea and Western India.

KEYWORDS

BSISO, Cyclones, ISO, LPS, Monsoon, MTCs, tropical convection

1 | INTRODUCTION

Extreme rainfall events in western India, particularly in the states of Maharashtra and Gujarat, are predominantly caused by mid-tropospheric cyclones (MTCs: Carr, 1977; Francis & Gadgil, 2006; Choudhury *et al.*, 2018; Kushwaha *et al.*, 2021, 2023). These MTCs are characterized by their peak intensity in the middle troposphere and relatively weak signatures in the lower troposphere. During the monsoon season, each MTC can cause heavy rainfall, with places like Mumbai and the Indian west coast often receiving over 500 mm of rain per event (Mapes, 2011; Choudhury *et al.*, 2018; Kushwaha *et al.*, 2023). Despite their significant contribution to the seasonal rainfall in this region and their crucial role in extreme rainfall events, the precise mechanisms behind the genesis of MTCs over the Arabian Sea and western India remain poorly understood.

Historical observations, particularly from the International Indian Ocean Expedition in July 1963, have provided essential insights into the key dynamic and thermodynamic conditions that prevailed during MTC genesis in the northern Arabian Sea (Miller & Keshavamurty, 1968). Notably, prior to MTC formation, a warm-core monsoon low-pressure system (LPS) developed in the Bay of Bengal and subsequently moved northwestward. There were also enhancements in cyclonic shear and a deepening of the middle troposphere trough around 600 hPa, extending from the Bay of Bengal to the Arabian Sea. Concurrent observations further highlighted the interaction between desert air and moist surface layers, evidenced by extensive stratocumulus clouds indicating moisture trapping under a strong temperature inversion caused by the advection of desert air over cooler marine air (Narayanan *et al.*, 2004; Someshwar Das *et al.*, 2007; Das *et al.*, 2021). This low-level temperature inversion was seen to dissipate with the MTC's intensification and played a significant role in controlling convection and middle tropospheric moisture during MTC formation.

A critical aspect of MTC genesis in July 1963 was the coexistence of a LPS over the Bay of Bengal and East India, which preceded the MTC and persisted during its development (Miller & Keshavamurty, 1968). This concurrent presence of the LPS has been observed in subsequent MTC events. Research indicates that a significant majority (90%) of heavy precipitating MTCs in Western India and the Arabian Sea are preceded by a Bay of Bengal LPS (Miller & Keshavamurty, 1968; Choudhury *et al.*, 2018). Furthermore, objective tracking and classification of MTCs have revealed that a substantial portion (83%) of in situ Arabian Sea MTC formation is linked to preexisting Bay of Bengal LPSs (Kushwaha *et al.*, 2023). In fact, the Arabian Sea MTCs that coexist with Bay of Bengal cyclonic systems represent the rainiest class of synoptic systems over Western India (Kushwaha *et al.*, 2023).

While prior studies have focused primarily on understanding the genesis of MTCs through the lens of barotropic and baroclinic instability of the mean flow and vorticity export theory (Mak, 1975; Mak *et al.*, 1982; Goswami *et al.*, 1980; Ramage, 1964), the dynamic interaction between the Bay of Bengal systems and Arabian Sea MTCs has not been explored extensively. Our study seeks to bridge this gap by employing a combination of observed concurrent MTC–LPS events from reanalysis data, complemented by numerical experiments using the Weather Research and Forecasting Model (WRF). We aim to investigate the dynamical connections between MTC formation in the Arabian Sea and LPS or cyclonic systems over the Bay of Bengal. A comprehensive understanding of this relationship is crucial for improving predictions of extreme rainfall events and for a deeper insight into the broader regional climate dynamics. The article is organized as follows: Section 2 details the data sources; Section 3 describes the methodology and the configurations of the WRF model; Section 4 presents an analysis of the meteorological field during the genesis of MTCs; Section 5 discusses the outcomes of our numerical simulations; and Section 6 offers concluding remarks and the implications of our findings.

2 | DATA

2.1 | NCEP final analysis data

The WRF model is configured to ingest various atmospheric datasets to produce the initial and boundary conditions. For this purpose, we utilize the widely used National Centers for Environmental Prediction Final Analysis (NCEP-FNL) Global Analysis dataset. FNL data are generated from the Global Data Assimilation System (GDAS), which uses observational data from the Global Telecommunications System (GTS) and other sources for assimilation. We utilized data at six-hourly intervals and one-degree horizontal resolution, available at https://rda.ucar.edu/datasets/ds083.2/. In fact, this is one of the most commonly used datasets for research and forecasting purposes (Kalnay *et al.*, 1996; Kesarkar *et al.*, 2007; Lo *et al.*, 2008; Melhauser & Zhang, 2012; Zhang *et al.*, 2011).

2.2 | ERA-5 reanalysis dataset

In this study, we utilize the fifth-generation atmospheric reanalysis, ERA-5, provided by the European Centre for Medium-Range Weather Forecasts (ECMWF) under the Copernicus Climate Change Service (C3S: Hersbach

et al., 2020). Containing a detailed record of the atmosphere, ocean, and surface from 1950 onwards, ERA-5 signifies several advancements over its predecessor, ERA-Interim, which was phased out in 2019. The ERA-5 reanalysis employs the Integrated Forecast System (IFS) version Cy41r2. Employing four-dimensional variational data assimilation, this model operates across 137 vertical levels and offers a resolution of 31 km (TL638 triangular truncation), a substantial enhancement compared with the 80-km resolution in ERA-Interim. With model outputs available hourly, ERA-5 significantly improves the representation of high-frequency variability and precipitation, facilitating more detailed evaluations of weather systems. To derive daily lag composites of various fields, we used winds, geopotential heights, specific humidity, and vorticity within the 1000 to 100 hPa layer. The analysis was performed at a spatial resolution of 1.5° and a daily temporal resolution.

2.3 | MTC–LPS events data

To examine comprehensively the observational aspects of interactions or connections between the cyclonic systems over the Bay of Bengal and coexisting MTCs, we utilize a dataset consisting of 59 instances of concurrent Arabian Sea MTCs and Bay of Bengal LPSs from 1998–2018 (Kushwaha *et al.*, 2023). This involved the use of 600-hPa geopotential height fields to detect and track cyclonic systems during these years. The cyclonic systems were then classified based on their genesis routes. In particular, we use the Type 2a subcategory from this dataset, which consists of instances where the Bay of Bengal systems coexisted with the Arabian Sea MTCs and where the genesis of Bay of Bengal LPSs preceded the formation of an MTC over the Arabian Sea.

3 | METHODOLOGY

3.1 | Bogus vortex scheme

To understand the effect of Bay of Bengal LPSs on the formation of Arabian Sea MTCs, we superimposed a cyclonic vortex over the Bay of Bengal as a perturbation to the June–July climatology of the NCEP Final Reanalysis. These modified data were used as initial conditions for the vortex initialization simulations. The construction of the vortex has been done using the National Center for Atmospheric Research (NCAR)–Air Force Weather Agency (AFWA) tropical cyclone (TC) "bogussing" scheme (Davis & Low-Nam, 2001; Fredrick *et al.*, 2009; Low-Nam & Davis, 2001). This method is not computationally expensive and follows the vorticity removal and inversion method to remove any preexisting vortex and insert a prescribed vortex in nonlinear balance. This method has been widely used as a "bogussing" scheme in the fifth-generation National Center for Atmospheric Research–Pennsylvania State University (NCAR–Penn State) Mesoscale Model (MM5) system. An updated version has been implemented in WRF (Davis *et al.*, 2002; Fredrick *et al.*, 2009). In particular, this method is widely utilized in enhancing the description and details of tropical cyclone initialization (Jian & Chun-Chieh, 2008) and in correcting the location and intensity of cyclone precursors (Ding *et al.*, 2004; Komaromi *et al.*, 2011; Kuester *et al.*, 2008; Van Nguyen & Chen, 2011; Wang *et al.*, 2008; Yang *et al.*, 2008). The scheme runs in two primary steps. The first step aims to find the background state by removing perturbed fields associated with the regional vorticity by solving a series of Poisson's equations. In the second step, a user-defined balanced vortex of prescribed winds and moisture profiles is placed in the specified location. Since our background state is already known as climatology, we only use the vortex addition part of the scheme. For further details of the method, please see Appendix A.

3.2 | Model setup

We utilize the WRF Model version 4 for our numerical experiments. Primarily, to understand the large-scale interactions between MTCs and Bay of Bengal LPSs, we have used a relatively coarse horizontal grid resolution of 57 km, along with 33 vertical hybrid sigma levels. First, we calculate climatology during June 20–July 10 using 16 years (2000–2015) of six-hourly FNL data; this part of the monsoon season has been chosen as most concurrent MTC–LPS events occur during late June and early July. This climatology serves as the background state for vortex addition. The 2000–2015 time interval is chosen for climatology as most of the input variables are consistent in dimensions and resolutions during this time, with notable differences in soil levels and vertical resolutions of the input data outside this window. Sea-surface temperature (SST) and soil moisture are maintained at their climatological values. Bogus vortices are added to the climatology in different locations over the Bay of Bengal to evaluate sensitivity and to reflect the variations in location of Bay of Bengal LPSs. Further, the FNL data provide specified lateral boundary conditions and initial conditions for dry and cold Bay of Bengal simulations.

TABLE 1 Model specifications.

S. No	Attribute	Attribute characteristic
1	Model	Weather Research And Forecast Model (WRFV4.0)
2	Model mode	Non-hydrostatic
3	Time step for integration	50 s
4	Number of domains	Single domain
5	Central point of the domain	20°N, 80°E
6	Horizontal grid distance (model grid resolution)	57 km
7	Map Projection	Mercator
8	Number of grid points	X-direction 100 Y-direction 68
9	Horizontal grid distribution	Arakawa C-grid
10	Nesting	No nesting
11	Vertical model level	Terrain-following hydrostatic-pressure coordinate (33 sigma levels up to 50 hPa)
12	Spatial differencing scheme	Sixth-order centered differencing
13	Initial condition	Three-dimensional real-data (1° × 1° FNL)
14	Lateral boundary conditions	WRF specified option
15	Time integration	Third-order Runge–Kutta
16	Microphysics	WRF single-moment 6-class scheme
17	Surface layer	MM5 similarity scheme
18	Planetary boundary layer (PBL)	Yonsei University Scheme (YSU)
19	Radiation	RRTMG shortwave and longwave schemes
20	Land-surface model	Unified Noah Land Surface Model
21	Cumulus parameterization schemes	New Tiedtke Scheme
22	Turbulence and mixing option	Evaluates second-order diffusion
23	Eddy coefficient option	Horizontal Smagorinsky first-order closure

As far as physics is concerned, several combinations of physics schemes can be used in the WRF; however, not all combinations are suitable for weather phenomena in different regions of the globe. Since Arabian Sea MTCs share similar characteristics with tropical systems (Kushwaha *et al.* 2021), we utilize a well-tested combination of physics for tropical systems known as the "TROPICAL SUITE" in our vortex addition experiments. A summary of important model details is presented in Table 1. The simulations are initialized with a Dolph digital filter, which runs backward and forwards for 12 h before the actual model runs, to remove any initial imbalances in the initial conditions (Peckham *et al.*, 2016). In the second set of experiments, the Bay of Bengal SST is cooled by replacing the SST over the Bay of Bengal with a cold Gaussian temperature distribution (see Appendix B for details), and the atmosphere is dried in the initial conditions over the Bay of Bengal and East India (see Figure S8 in the Supporting Information). After trial and error, a slightly different combination of physics schemes is used, which reproduces the intensity, size, and location of the simulated July 2020 MTC satisfactorily compared with observations. In particular, for cumulus parameterization, we use the Kain–Fritsch scheme; the Kessler scheme is used for microphysics, with other schemes from the "CONUS SUITE", specifically RRTMG for radiation, the Mellor–Yamada–Janjic scheme (MYJ) for the planetary boundary layer, Eta Similarity Scheme for the surface layer, and Unified Noah Land Surface Model for land-surface parameterization.

3.3 | Vorticity budget

To understand the intensification of Arabian Sea MTCs, we use a vorticity budget (Boos *et al.*, 2015a; Holton, 1973;

Raymond *et al.*, 2011). The inviscid vertical relative vorticity (ξ) budget equation in pressure coordinates reads

$$\frac{\partial \xi}{\partial t} = -\xi \nabla.\mathbf{V} - f\nabla.\mathbf{V} - \mathbf{V}.\nabla\xi - \beta v - \omega\frac{\partial \xi}{\partial p} + \left(-\frac{\partial \omega}{\partial x}\frac{\partial v}{\partial p} + \frac{\partial \omega}{\partial y}\frac{\partial u}{\partial p}\right) + \text{Res.} \quad (1)$$

In the equation, ξ represents relative vorticity, β the meridional gradient of the Coriolis parameter, ω the vertical pressure velocity, u the zonal wind component, v the meridional winds, and $\mathbf{V}$ the total wind vector. The first two terms on the right-hand side (RHS) represent vorticity generation (destruction) by convergence (divergence) of horizontal winds when coupled with relative and planetary vorticity, respectively. The third term represents vorticity advection by the horizontal wind ($\mathbf{V}$), the fourth term is the coupling between differential planetary vorticity and meridional wind (the so-called β-term), the fifth term represents the vertical advection of relative vorticity via upward or downward motion, and the sixth term is the tilting or twisting term, which is the change in vorticity due to horizontal gradients in the vertical velocity or vice versa. Finally, the last term is a residual that arises due to parameterized physics and numerical approximations in post-processing the data. To understand the formation and intensification of MTCs, each term of the vorticity equation is calculated and compared in order to deduce the dominant contributions to system growth.

4 | BAY OF BENGAL LPSS AND GENESIS OF MTCS OVER ARABIAN SEA

We commence our analysis by examining the observational aspects of the genesis of MTCs over the northeastern Arabian Sea during the prevalence of a cyclonic system in the Bay of Bengal. Specifically, we utilize data from 59 instances where the genesis of MTCs over the northeastern Arabian Sea was preceded by the formation of a cyclonic system in the Bay of Bengal. These instances are defined as Type 2a MTCs (Kushwaha *et al.*, 2023).

Plan views of Type 2a MTC daily lag composites, including anomalies of total precipitable water, relative vorticity, and geopotential height, along with wind vectors, are shown in Figure 1 in rows 1, 2, and 3, respectively. Where applicable, variables are vertically averaged between 800 and 400 hPa to ensure that the composite anomalies have a coherent vertical structure and are robust throughout the depth of the middle troposphere. The horizontal extent and magnitude of precipitable water anomalies (row 1; Figure 1) increase over the northeastern Arabian Sea from Day −6 to Day 0, that is, until the day of heaviest precipitation. During this period, the wind anomaly (quivers in Figure 1) is easterly and slightly northeasterly over the northern Arabian Sea, where the maximum accumulation of water vapor is observed. The easterly wind anomalies are not localized to the Arabian Sea region but appear as part of a large-scale circulation; indeed, wind anomalies originate from the Bay of Bengal and extend to the Arabian Sea, enveloping the southern peninsula of India.

Sequentially, on Day −6, a weak negative height anomaly envelops the southern tip of India (row 3; Figure 1), accompanied by a slight positive vorticity anomaly over the southwest Bay of Bengal (around 15°N, 85°E; row 2, Figure 1). The height anomaly over the Arabian Sea exhibits a large-scale east–west oriented structure, restricted to the south of 15°N (row 3; Figure 1). The Bay of Bengal height anomaly, centered near 15°N–85°E, deepens from Day −6 to Day −4, with an intensification of associated relative vorticity anomalies (row 2 of Figure 1). Following this, an east–west shear zone forms, extending from the Bay of Bengal to the Arabian Sea (rows 2 and 3; Days −6 to −2; Figure 1). Within this evolving shear zone, over the Arabian Sea, as seen on Day −4, two significant positive relative vorticity anomaly centers form—one near the west coast of India, near 15°N and 72°E, and another around 65°E and 18°N. With the further intensification of the system over the Bay of Bengal (Days −4 to −2), the westward-situated Arabian Sea vorticity anomaly moves eastward, and by Day −2 it merges with the anomaly over the western coast of India. As the height anomaly over the Bay of Bengal deepens and moves northward (Day −6 to Day −2), the trough over the Arabian Sea intensifies and becomes more localized off the coast of Maharashtra. This is reflected in the rapid increase of vorticity anomalies over the northeastern Arabian Sea from Day −2 to Day 0 (row 2; Figure 1).

Overall, the evolution of 600-hPa geopotential height, velocity fields, and wind anomalies suggests that the dynamic state of the atmosphere over the Arabian Sea and western India is indeed linked with the Bay of Bengal system during Type-2a MTC formation. However, the first geopotential height anomalies deepen and vorticity intensifies over the Bay of Bengal, followed by an increase in vorticity over the Arabian Sea. The intensification of the Bay of Bengal system before that of the Arabian Sea region seems reasonable, as, during the primary monsoon months, the Bay of Bengal's SST and precipitable water are relatively high compared with those of the Arabian Sea (Masunaga, 2014; Saikranthi *et al.*, 2019a, 2019b). These conditions are favorable for the development and intensification of cyclonic systems. Conversely, deep

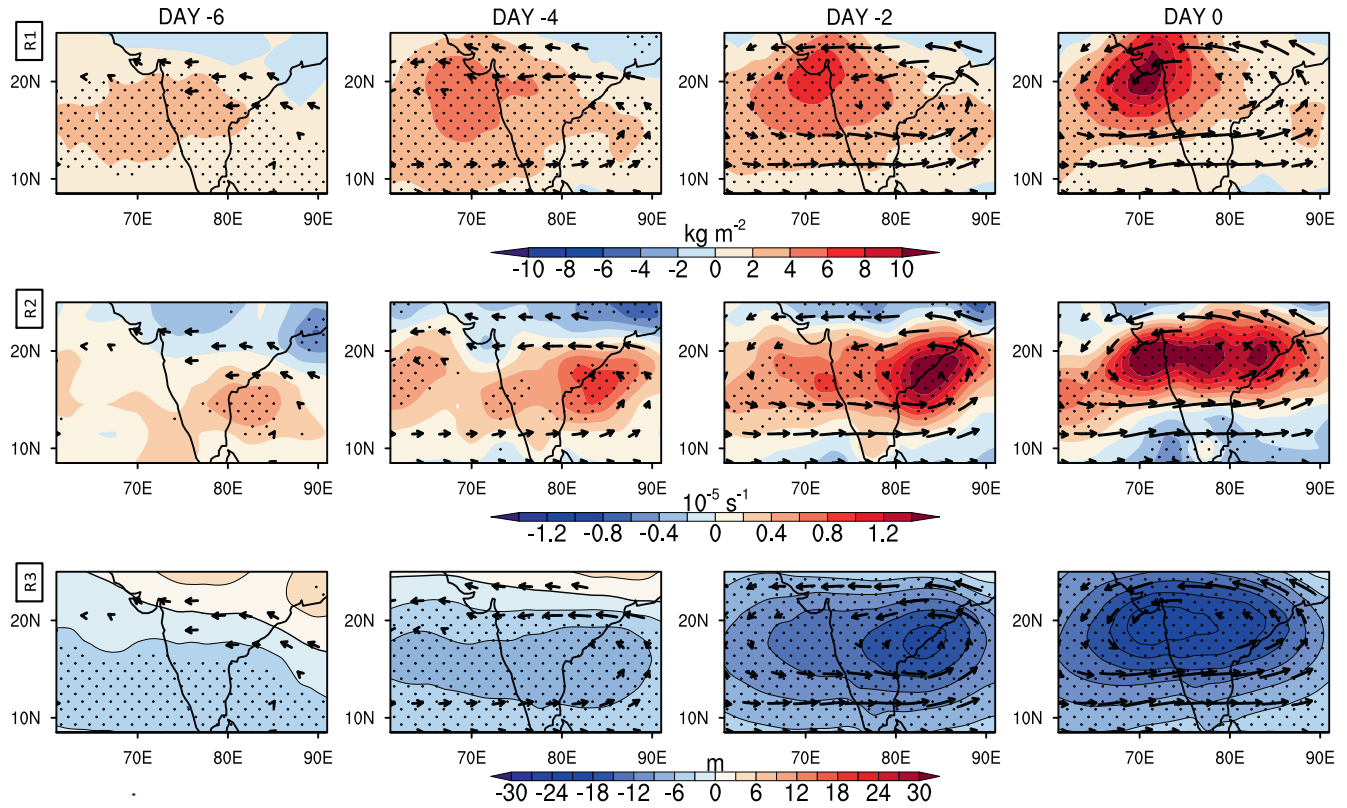

FIGURE 1 Lag composite of 59 Type 2a systems (Kushwaha *et al.*, 2023), averaged over the 800–400 hPa layer and extending from Day −6 to Day 0. Day 0 is defined as the day of maximum precipitation during the lifespan of the MTC. This figure showcases anomalies in precipitable water (Row 1: R1), relative vorticity (Row 2: R2), and geopotential height (Row 3: R3). The dotted region highlights areas where the fields differ significantly from zero at a 0.1 significance level. Wind vectors are included only if any component of the wind significantly deviates from zero at a 0.1 significance level, as determined by a two-tailed Student's *t*-test. The anomalies are calculated based on the daily climatology from 1998–2018. For ease of comparison, June–September climatology during 1998–2018 for different variables is shown in Figure S12. [Colour figure can be viewed at wileyonlinelibrary.com]

convection over the Arabian Sea is usually hampered by colder SSTs due to the upwelling of subsurface cold water, exacerbated further by a dry middle troposphere and a low-level inversion (Das *et al.*, 2021; Muraleedharan *et al.*, 2013; Narayanan *et al.*, 2004). Furthermore, the composite Type 2a MTC circulation and geopotential height anomaly distribution at 600 hPa (as shown in row 3 of Figure 1) are characterized by a zonally oriented trough. The associated circulation originates in the Bay of Bengal and extends to the Arabian Sea. Additionally, the height anomalies of the Bay of Bengal system are non-circular and extend westward, aligning with the zonal trough. This trough is remarkably similar to the steady-state Rossby response to off-equatorial heating (Gill, 1980; Goswami, 1987). Thus, the apparent atmospheric link between the Arabian Sea and the Bay of Bengal basins may be mediated by the Gill response (Gill, 1980) to off-equatorial diabatic heating over the Bay of Bengal and East India. Previous studies have noted the remote influence of Bay of Bengal heating on western Indian circulation, wherein cyclonic vorticity and precipitation over western India and the northeastern Arabian Sea were enhanced when heating was prescribed over the Bay of Bengal, argued to be due to a Rossby-wave response to the heating (Choudhury *et al.*, 2018; Xie *et al.*, 2006). More broadly, the remote induction of synoptic-scale systems downstream of a mature tropical cyclone has been observed in various ocean basins (Krouse & Sobel, 2010; Schenkel, 2016, 2017), including cyclogenesis in Rossby waves radiated from a parent cyclone (Krouse *et al.*, 2008).

Up to now, we have focused on the horizontal evolution of the system; to understand the vertical structure evolution of dynamical fields during the formation of Type 2a systems, vertical–horizontal cross-sections of composite anomalies of relative vorticity, zonal winds, and specific humidity anomalies of 59 Type 2a MTCs are shown in Figure 2. Before Day −4 (not shown), the relative vorticity was disorganized and weak in much of the troposphere over western India. However, as soon as the low-level relative vorticity anomalies spin up over the Bay of Bengal, the corresponding mid- to low-level entities

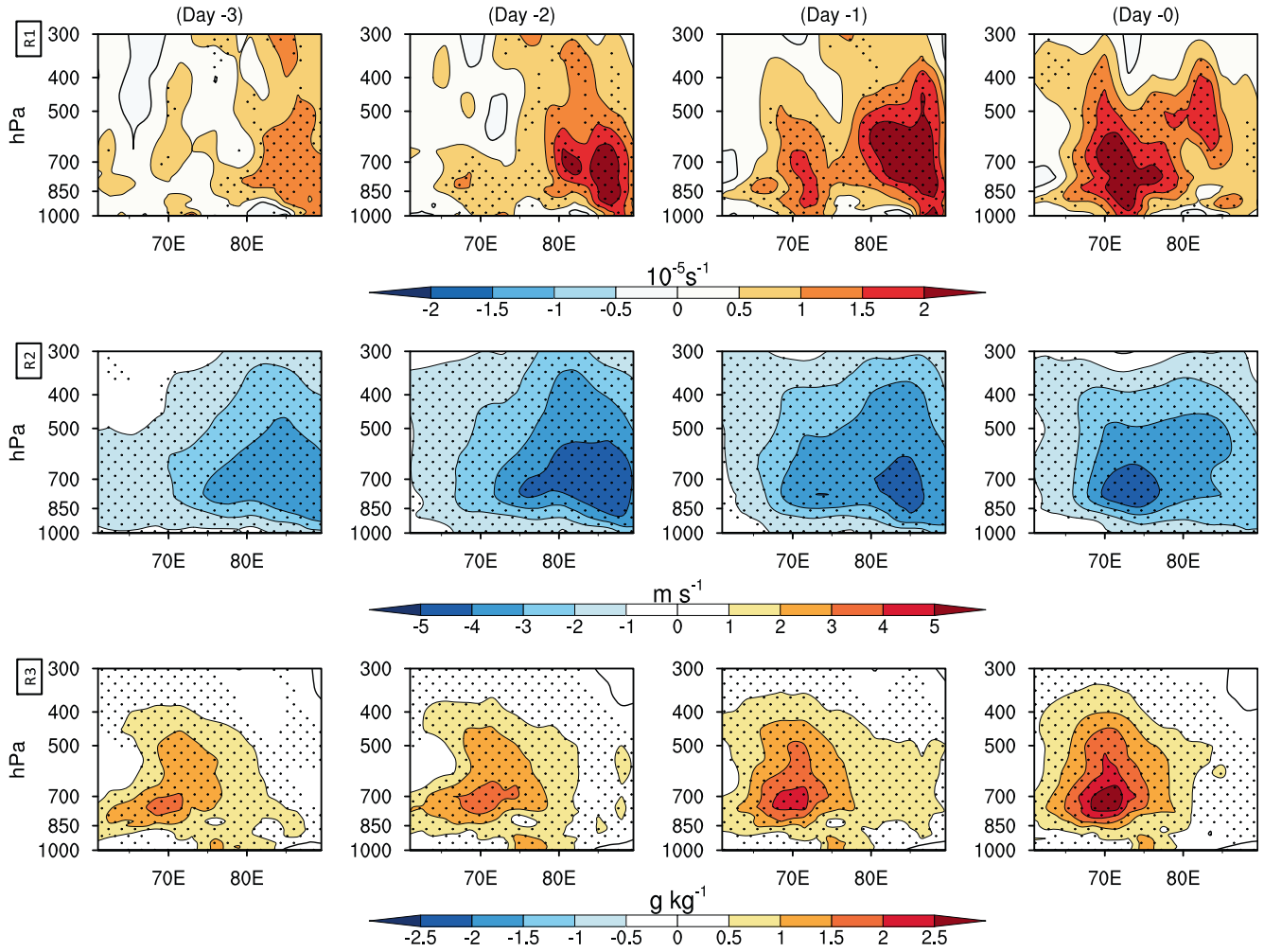

FIGURE 2 A cross-section of lag composites of 59 Type 2a MTCs spanning from Day −3 to Day 0 (Kushwaha *et al.*, 2023). Day 0 corresponds to the day of maximum precipitation during the lifespan of the composite MTCs. Row 1 (R1) displays the relative vorticity anomaly, with a cross-section at 18.5°N. Row 2 (R2) shows the zonal wind anomaly, with a cross-section at 22°N. Row 3 (R3) depicts the specific humidity anomaly, with a cross-section at 18.5°N. Regions of significance are shaded to indicate a 0.1 significance level under a two-tailed Student's *t*-test. The anomalies are calculated based on the daily climatology from 1998–2018. For ease of comparison, June–September climatology during 1998–2018 for different variables is shown in Figure S12. [Colour figure can be viewed at wileyonlinelibrary.com]

increase in an organized and statistically significant manner over the Arabian Sea (Figure 2; rows 1 and 2). In the later stages (Day −1 to 0), the vorticity anomalies mostly remain confined to and intensify in the lower levels, reflecting the increasing presence of deep convection in the system (Kushwaha *et al.*, 2021; Murthy & Boos, 2019; Russell & Aiyyer, 2020).

The zonal wind (second row; Figure 2) shows a significant increase in an easterly wind anomaly in the middle troposphere from Day −3 to Day −1 over western India, which extends up to 300 hPa with a maximum around 700 hPa. Thus, a comparison of wind anomalies in Figures 1 and 2 suggests that the anomalous easterlies in the middle troposphere over the Arabian Sea are linked to the system in the Bay of Bengal. These enhanced easterlies help prevent dry-air mixing from the north and west and decrease the strength of the inversion by reducing elevated warm-air advection (Dwivedi *et al.*, 2021; Narayanan *et al.*, 2004). This is reflected precisely as a significant increase in specific humidity anomalies (Figure 2, row 3: R3) from 850 to 400 hPa over western India (around 70°E). These favorable conditions allow for the development of deep convection and help moisten the free troposphere over the Arabian Sea further. The increase in the strength of the anomalous easterlies and their influence is more clearly evident in Figure 3. From Day −6 to Day 0, middle tropospheric easterlies become stronger (Figure 3a) and, concomitantly, relative humidity increases over western India (Figure 3b). The expected reduction in low-level static stability or reduction in strength of the low-level inversion is also observed (Figure 3c). A weaker inversion allows for an increase

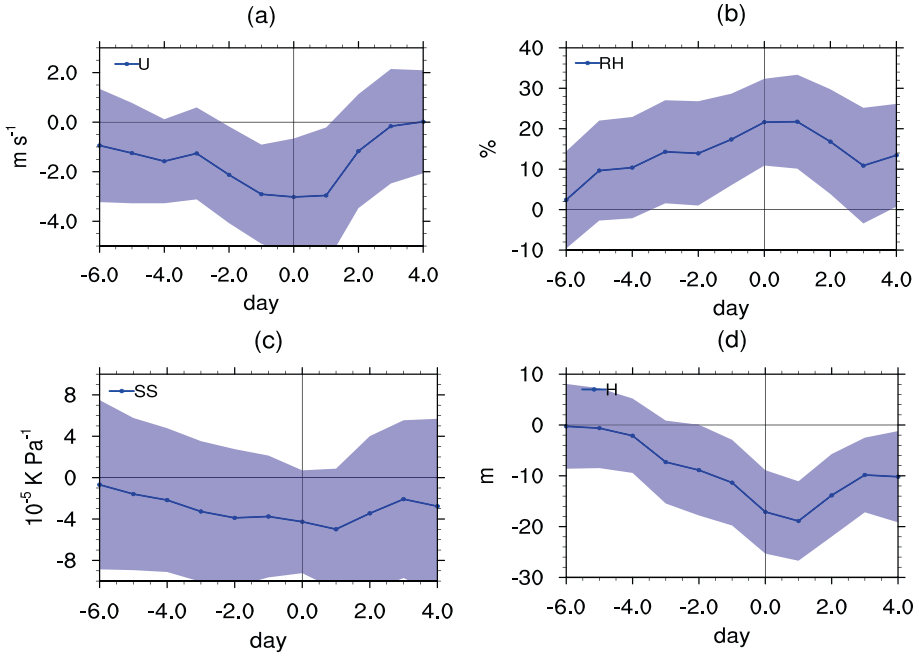

FIGURE 3 The lag composite time series of 59 Type 2a MTCs (Kushwaha *et al.*, 2023), at 22°N and 72°E, spans from Day −6 to Day 4. Day 0 corresponds to the day of maximum precipitation during the lifespan of the MTC. The panels illustrate (a) zonal wind anomalies in $m \cdot s^{-1}$, averaged between the 650–550 hPa levels; (b) relative humidity anomalies averaged within the 650–550 hPa layer; (c) static stability parameter anomalies, averaged in the 700–800 hPa layer, expressed as (10^{-5} $K \cdot Pa^{-1}$); and (d) height anomalies in m at the 500 hPa level. Shadings indicate the ranges of one standard deviation. The anomalies are calculated based on the daily climatology from 1998–2018. [Colour figure can be viewed at wileyonlinelibrary.com]

in middle troposphere moisture, which favors deep convection (Raymond *et al.*, 2015) and further spins up an MTC, deepening the height anomaly as seen in Figure 3d.

To a first approximation, we hypothesize that sufficient latent heating in the atmosphere above the Bay of Bengal and East India results in an off-equatorial Gill-type response, consisting of a westward-extending zonal trough that reaches up to the Arabian Sea, starting from the Bay of Bengal (Choudhury *et al.*, 2018; Gill, 1980; Goswami, 1987; Xie *et al.*, 2006). Given its rotational character, this Rossby gyre is characterized by enhanced horizontal shear and cyclonic vorticity over western India. A similar response to realistic diabatic heating in the middle troposphere has been noted in recent general circulation model experiments (Choudhury *et al.*, 2018; Xie *et al.*, 2006). Moreover, the enhanced horizontal shear associated with the Rossby gyre can be critical for the growth of the Arabian Sea system through barotropic instability (Goswami, 1987; Goswami *et al.*, 1980); in fact, moist barotropic instability has been identified as a possible source of energy for the formation of monsoon lows and MTCs (Diaz & Boos, 2019a, 2019b; Goswami *et al.*, 1980). In addition to the shear and vorticity, the enhanced easterlies north of the northeastern Arabian Sea and western India prevent the inflow of desert air, thus weakening the climatological inversion and raising the possibility of convection that can moisten the free troposphere. The altered dynamic and thermodynamic conditions, forced by LPS-induced heating in the Bay of Bengal and East India, in turn favor the formation of MTCs over the northeastern Arabian Sea and western India.

5 | BOGUS LPS OVER THE BAY OF BENGAL

To verify the hypotheses suggesting that systems in the Bay of Bengal influence the Arabian Sea environment significantly and subsequently contribute to the genesis of MTCs, we conducted a series of numerical experiments using the WRF model. The model's configuration, setup, and the application of the bogus vortex technique are detailed in Section 3. The model domain, encompassing several key components of the monsoon such as the Somali Jet, the monsoon trough, the heat low, and both the Bay of Bengal and the Arabian Sea, is depicted in Figure 4.

In the first set of experiments, 21 bogus vortices or LPSs were introduced over various locations in the Bay of Bengal (Figure 4). Particular attention was given to region A1, where nine bogus vortices (with $r_m = 350$ km, $v_{max} = 14\ m \cdot s^{-1}$ or 27 kt) were placed (at coordinates 14°N, 81°E; 15°N, 81°E; 16°N, 81°E; 14°N, 82°E; 15°N, 82°E; 16°N, 82°E; 14°N, 83°E; 15°N, 83°E; 16°N, 83°E). This region is significant, as it is where the first signs of LPS emerge on Day −6 in the composite plan views of Type 2a formation (Figure 1). The remaining 12 members were distributed across regions A2– A4.[1] Specifically, the coordinates in region A2 are 18°N, 81°E; 18°N, 83°E; 20°N, 81°E; 20°N, 83°E; in region A3 they are 18°N, 85°E; 18°N, 87°E; 20°N, 85°E; 20°N, 87°E; and in region A4 they are 14°N, 85°E; 14°N, 87°E; 16°N, 85°E; 16°N, 87°E. We used slightly reduced vortex sizes of $r_m = 200$ km in regions A2, A3, and A4 (compared with $r_m = 350$ km in A1) to mitigate model instabilities caused by the Himalayan topography at higher latitudes during dynamical adjustment. In

A1, more realistic vortex sizes were maintained, as this is where monsoon lows first appear in observations in the Bay of Bengal (Figure 1). Additionally, all vortices were set to a strength of $v_{max} = 14\,m{\cdot}s^{-1}$ or 27 kt, corresponding to the strength of a monsoon depression as defined by the India Meteorological Department (IMD).

The 600-hPa geopotential height, after 24 h of simulation for the nine members of group A1, is shown in Figure S1 in the Supporting Information. Consistently, every ensemble member exhibits areas of low geopotential height at the locations where the bogus vortices were introduced. This is accompanied by a trough extending from the Bay of Bengal to the Arabian Sea and western India. Notably, apart from this trough, there is no indication of MTCs over the Arabian Sea. However, the 600-hPa heights after 60 h of model integration (Figure 5) suggest the presence of MTCs. This is evidenced by the closed height contours centered around 70°E and 18°N in all nine ensemble members of region A1. Figure S3 illustrates the entire formation cycle of an MTC in a single ensemble member introduced at 82°E and 15°N (center of region A1). It is important to note that a similar evolution is observed in other ensemble members (not shown). The time evolution clearly demonstrates that as the Bay of Bengal system progresses northward, the associated height perturbations extend westward. This results in a westward-extending zonal trough covering parts of western India and the Arabian Sea from 24–36 h. Within the western end of this trough, which extends over portions of the Arabian Sea, a closed vortex emerges after approximately 48 h of simulation and reaches maturity as a closed vortex around 60 h.

Furthermore, this zonal trough connects the induced MTC with the bogus Bay of Bengal vortex. Both systems encircle each other in a manner similar to Type 2a composites (see Figure 1) and align with specific MTC observations (Miller & Keshavamurty, 1968). A careful

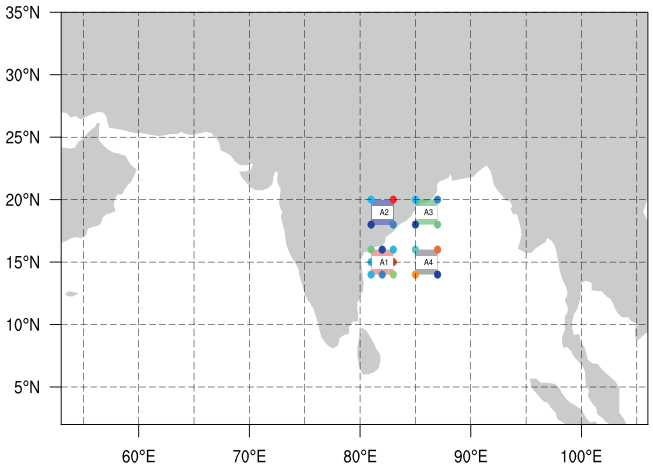

FIGURE 4 The model domain, with locations marked for 21 bogus vortices divided into four sets: A1, A2, A3, and A4. Group A1 comprises nine members, while groups A2–A4 consist of four members each. [Colour figure can be viewed at wileyonlinelibrary.com]

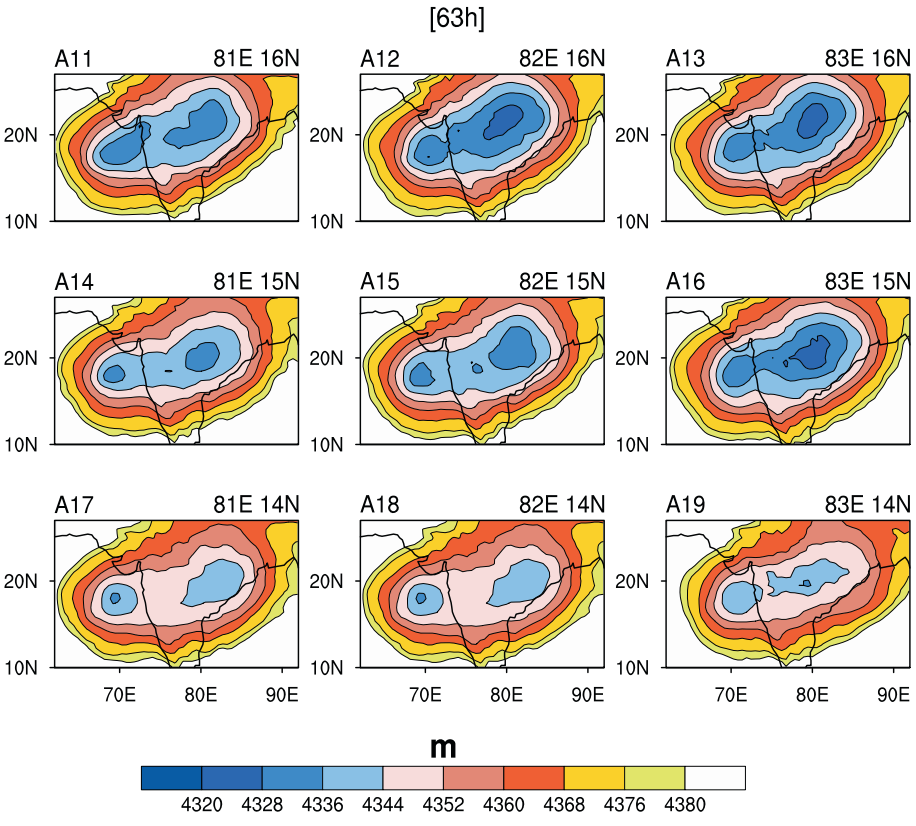

FIGURE 5 Geopotential height at 600 hPa for the nine members (A11–A19) of group A1 after 63 h of simulation. Each subplot represents the height fields of the respective vortex located at nine different positions. [Colour figure can be viewed at wileyonlinelibrary.com]

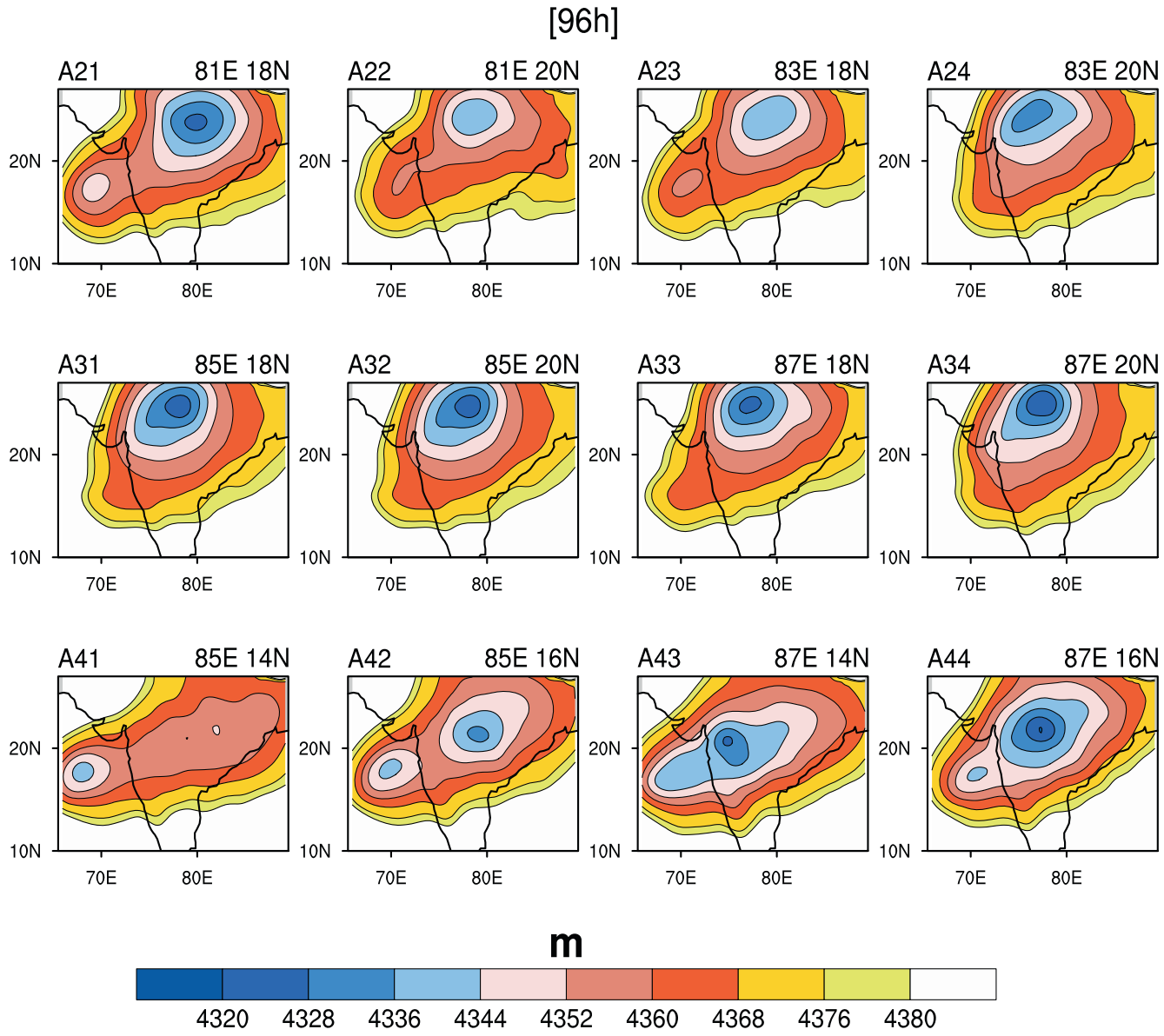

FIGURE 6 The geopotential height at 600 hPa for 12 members of group A2 (row 1), group A3 (row 2), and group A4 (row 3) after 96 h of simulation, respectively. Each subplot in the rows represents the height fields of the respective vortex located at four different positions. [Colour figure can be viewed at wileyonlinelibrary.com]

examination of the location of the trough and the MTC formation site in Figures S1, S3, and 5, respectively, suggests that MTC formation occurred in the middle tropospheric trough induced by the bogus Bay of Bengal vortex.

To understand the sensitivity of MTC genesis to different locations of Bay of Bengal LPSs, other ensemble members were added over regions A2, A3, and A4, as shown in Figure 4. The 600-hPa geopotential surface after 24 h of model integration for groups A2–A4 is shown in Figure S2. During the first 24 h of simulation, similar to group A1, we observe only a westward-extending trough up to the Arabian Sea without the formation of a closed vortex or the existence of an MTC. However, after 96 h of model integration, the formation of MTCs becomes evident over the Arabian Sea and western India in groups A2 (as shown in the first row of Figure 6) and A4 (depicted in the third row of Figure 6). In contrast, for most members of set A3 (illustrated in the second row of Figure 6) we observe a relatively short and less zonally oriented trough formation. Notably, the trough formation in A3 members does not evolve into a closed-form vortex or MTC within the 96 hours of model integration. This sensitivity may be attributed to the specific location of the initial vortices in region A3, which are the most northeast among all groups. This observation aligns with the findings of Kushwaha *et al.* (2023), who demonstrated that the majority of in situ MTCs are associated with Bay of Bengal

LPSs that follow a relatively southern track, while most LPSs taking relatively northern tracks are usually not connected to rainy MTCs over the Arabian Sea. These results strongly support the hypothesis that a robust dynamic link exists between Bay of Bengal LPSs with relatively southern tracks and the genesis of Type 2a MTCs over the Arabian Sea and Western India. Remarkably, when a bogus vortex is introduced to the climatological conditions in favorable locations over the Bay of Bengal, an MTC is triggered over western India or the Arabian Sea within a timeframe of 60–100 h (2.5–4 days), clearly highlighting the significant influence of the Bay of Bengal systems.

5.1 | Vorticity budget

The genesis of MTCs in all the ensemble members from region A1 raises the question of which terms in the vorticity budget are dominant in contributing to the growth of the cyclonic system over the Arabian Sea and western India. The composite time series of various terms in the vorticity budget (details of which are in Section 3), averaged over the MTC region (15–20°N, 65–72°E) between 550 and 650 hPa, is depicted in Figure 7. The calculated vorticity tendency (Figure 7a, green curve) and the sum of all terms on the right side of the vorticity budget (Equation 1: Figure 7a, blue curve) align closely, suggesting an approximate closure of the vorticity budget. Notably, in the first 24 h of simulation, the positive vorticity tendency is driven primarily by advection (mainly the β-term) and tilting terms (Figure 7a,b).

During the initial 24 h, the stretching term does not contribute significantly. However, the vorticity tendency increases rapidly after this period, reaching a peak around 70 h. In contrast to the first 24 h, vortex stretching accounts primarily for the intensification from 24 to 72 h (Figure 7a, red curve). Moreover, the coupling of relative vorticity with divergence contributes a slightly larger portion to the stretching than the coupling of planetary vorticity with divergence (not shown). Meanwhile, during the same period, horizontal advection of vorticity (Figure 7a, black curve) acts as a significant sink, opposing vortex stretching. Although the β-term (Figure 7b, green curve) is dominant during the first 24 h and continues as a mild vorticity source throughout the MTC formation, it remains relatively small compared with the stretching term during the rapid intensification phase (24–70 h). The vertical advection of vorticity (Figure 7b, red curve) also serves as a vorticity source in the 550–650 hPa layer; however, it peaks after the maximum of $\partial\xi/\partial t$, suggesting a minimal contribution during the rapid growth phase of the MTC (around 70 h). The peak of the vertical advection term after the maximum intensification rate of the mid-level maximum (compare green and red curves in Figure 7b) indicates a shift of the MTC vorticity maximum to the lower levels (see, for instance, the LTC phase, Kushwaha *et al.*, 2021).

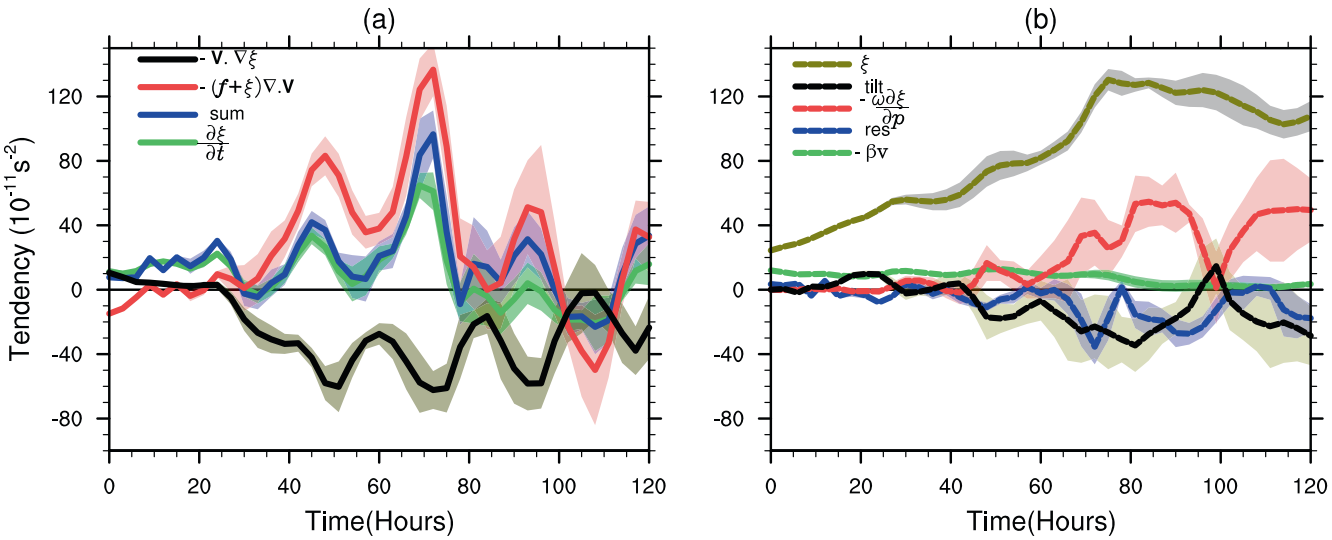

FIGURE 7 Composite time series of various terms in the vorticity budget of ensemble A1, averaged over the MTC region (15–20°N, 65–72°E) between 550 and 650 hPa. Panel (a) shows the calculated composite vorticity tendency (green), the sum of the RHS of the vorticity equation (blue), advection of vorticity (black), and the stretching term (red). Panel (b) presents the relative vorticity (dark green), tilting term (black), vertical advection of vorticity (red), residual term (blue), and the beta term (green). The time axis corresponds to simulation time. The units of vorticity tendency terms are 10^{-11} s^{-2}. For comparison, the relative vorticity, ξ, in Figure 7b is multiplied by 2×10^{-6}; hence, its units are 0.5×10^{-6} s^{-1}. Shading represents one standard deviation among A1 ensemble members. In panel (b), the legend "res" represents the residual in the vorticity budget, while "tilt" stands for the tilting term. [Colour figure can be viewed at wileyonlinelibrary.com]

This shift can lead to positive vertical advection of relative vorticity from the lower to the middle troposphere in an environment of upward wind velocity.

To understand the spatial distribution of various terms in the vorticity budget, a plan view of the vorticity budget during the initial 24 h is shown in Figure 8. The vorticity tendency ($\partial\xi/\partial t$; Figure 8g) matches the sum of all terms on the right side of the vorticity equation (Figure 8h), suggesting an approximate spatial closure of the vorticity budget. Two centers of positive vorticity tendency are observed: a strong one over the Bay of Bengal and East India, related to the intensification of the bogus LPS, and another relatively weaker maximum over the northeast Arabian Sea off the coast of Mumbai, linked to the incipient MTC. Consistent with the time series in Figure 7, during the first 24 h, the total positive vorticity tendency over the Arabian Sea (Figure 8h) results mainly from the tilting term (Figure 8e), the β-term (Figure 8f), and advection of relative vorticity (Figure 8c). The β-term (Figure 8f) shows a broad positive tendency over the Arabian Sea in

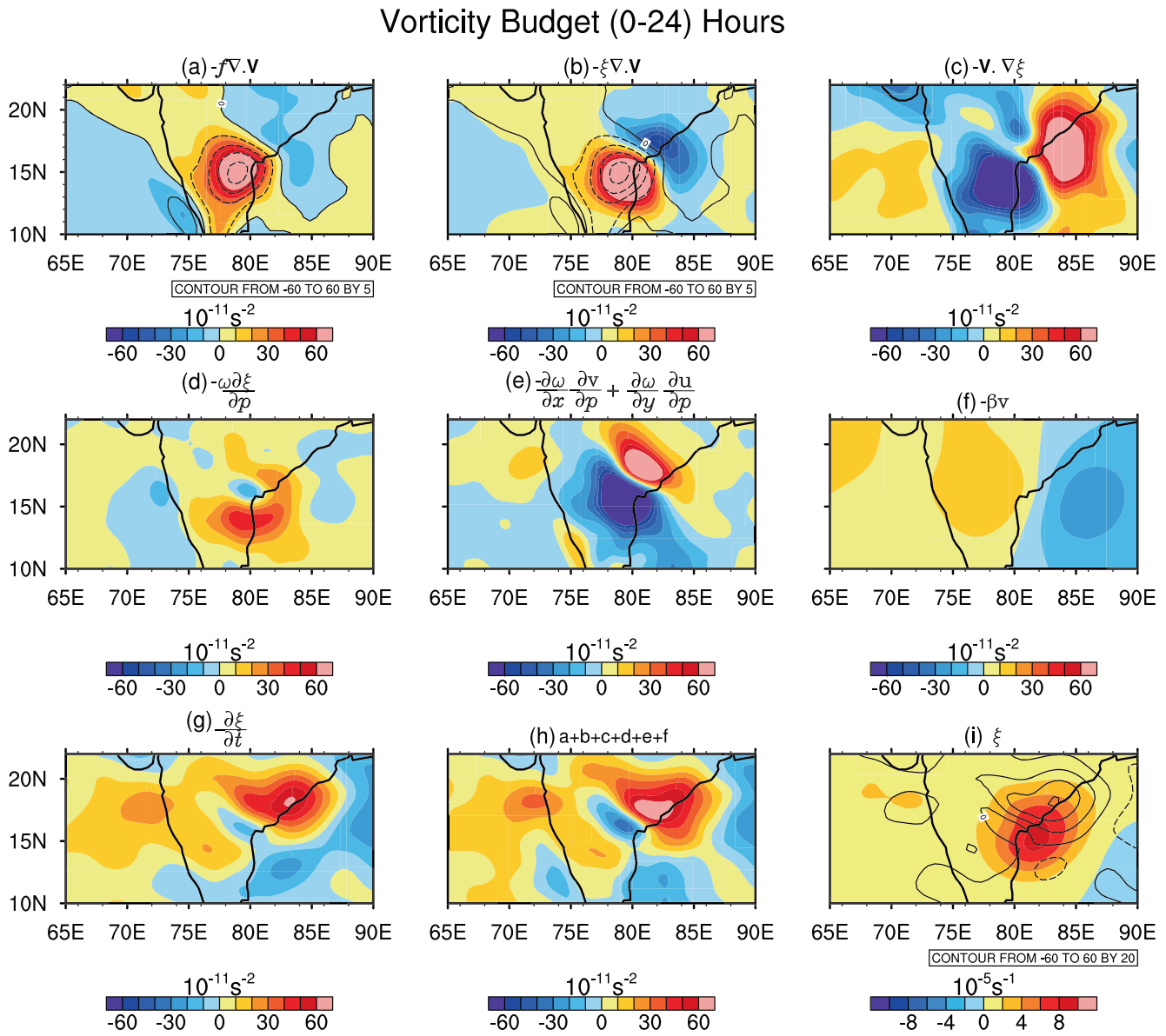

FIGURE 8 Plan view of various terms in the vorticity budget of ensemble A1, averaged between 550 and 650 hPa and over the first 24 h of simulation. Panel (a) represents the stretching term as a part of planetary vorticity; (b) shows the stretching term as a part of relative vorticity; (c) displays the advection of vorticity by horizontal winds; (d) illustrates the advection of vorticity by vertical winds; (e) demonstrates vorticity generation by tilting; (f) represents the beta term; (g) displays the calculated vorticity tendency; (h) shows the sum of the right-hand side of the vorticity Equation 1; and (i) depicts relative vorticity (shaded areas) overlying vorticity tendency (contours). In (a) and (b), dashed and solid contours represent convergence and divergence, respectively. Symbols have their usual meanings. [Colour figure can be viewed at wileyonlinelibrary.com]

regions of southerly winds in the western sector of the vortex or LPS. The stretching term (Figure 8a,b) remains positive over western India; however, it contributes less relative to tilting (Figure 8e) and advection of absolute vorticity (Figure 8c,f). Notably, vertical advection (Figure 8d) does not appear to be a major source of vorticity during the first 24 h over the Arabian Sea. Additionally, the vorticity maxima (Figure 8i, shaded areas) are nearly over the same region where the vorticity tendency is also positive (Figure 8i, contours), suggesting the formation of an intensifying vortex. Thus, during the initial phase of the genesis of the MTC, the advection of absolute vorticity and tilting of the horizontal vorticity vector by the horizontal gradients of the vertical motion explain almost the entire geographical distribution of the vorticity tendency.

The plan view of the vorticity budget during 24–48 h of model integration is shown in Figure 9. The pattern of observed vorticity tendency (Figure 9g) and the sum of the right-hand side of the vorticity equation (Figure 9h) show a similar magnitude and horizontal distribution, again

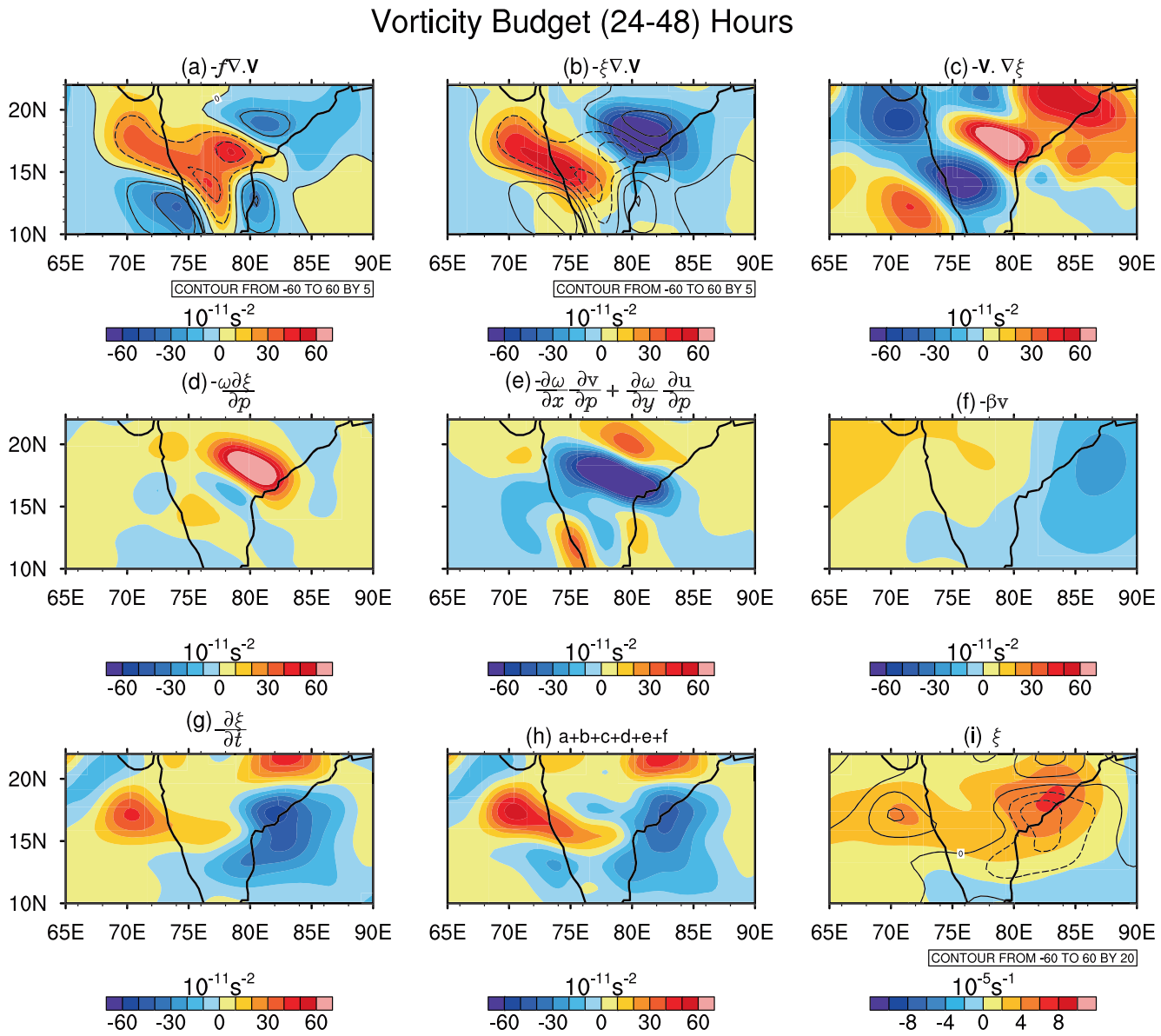

FIGURE 9 Plan view of various terms in the vorticity budget of ensemble A1, averaged between 550 and 650 hPa and averaged over 24–48 h of simulation. Panel (a) represents the stretching term as a part of planetary vorticity; (b) shows the stretching term as a part of relative vorticity; (c) displays the advection of vorticity by horizontal winds; (d) illustrates the advection of vorticity by vertical winds; (e) demonstrates vorticity generation by tilting; (f) represents the beta term; (g) displays the calculated vorticity tendency; (h) shows the sum of the right-hand side of the vorticity Equation 1; and (i) depicts relative vorticity (shaded areas) overlying vorticity tendency (contours). In (a) and (b), dashed and solid contours represent convergence and divergence, respectively. Symbols have their usual meanings. [Colour figure can be viewed at wileyonlinelibrary.com]

suggesting a sufficiently balanced budget. In contrast to the budget during the first 24 h, the total vorticity tendency during 24–48 h is explained almost entirely by the total stretching term (Figure 9a,b). However, note that though the total tendency follows stretching, advection acts to cancel it and reduces its effectiveness in the intensification process. The opposing nature of stretching and advection, and their almost cancellation, has also been observed in the movement of monsoon depressions (Boos *et al.*, 2015b). The β-term (Figure 9f) and vertical advection (Figure 9d) act as a source; however, their magnitudes are much lesser than that of the stretching term. In contrast to the first 24 h, here the advection of relative vorticity by horizontal winds (Figure 9c) and the tilting term (Figure 9e) act to damp the vorticity tendency. The total vorticity tendency (Figure 9i, contours) and regions of positive vorticity maximum (Figure 9i, shaded areas) almost overlap, suggesting that the vorticity tendency contributes primarily to the intensification, and not much to the motion of the incipient MTCs—in accord with the observations of the quasi-stationary nature of Type 2a MTCs (Carr, 1977; Kushwaha *et al.*, 2021, 2023). To a large extent, these characteristics align with the vorticity budget of the July 1963 MTC, which identified stretching as the primary source, followed by vertical advection and the β-term, while advection acted as the main sink of vorticity (Carr, 1977). Consistently, the vorticity budget of individual MTCs in the ERA-5 reanalysis also identifies vortex stretching as the major source and advection as the primary sink of vorticity during the rapid intensification phase (Figures S4–S7). Overall, the vorticity budget suggests that the advection of absolute vorticity and tilting initially provide a positive vorticity environment conducive to MTC growth. However, during the rapid intensification phase, vorticity stretching becomes the dominant factor in MTC intensification.

Furthermore, as demonstrated in Figures 1 and 2, the anomalous easterly winds from the Bay of Bengal converge over the Arabian Sea. These middle-level anomalous easterlies play a crucial role; they reduce desert air intrusions from the west and north, weaken the inversion layer, create favorable conditions for convection, and contribute to the moistening of the middle troposphere. This important role of the easterlies is confirmed further in the model runs for group A1, as depicted in Figure 10.

Specifically, Figure 10a,b clearly illustrates that from −40 h to the rapid intensification phase (i.e., before hour 0), both the static stability (Figure 10a) and the strength of the inversion layer (Figure 10b) decrease continually in the lower troposphere. Concurrently, the relative humidity increases (Figure 10c), reaching near-saturation just prior to maximum intensification. Mirroring the observations (Figure 3), both the simulated static stability parameter

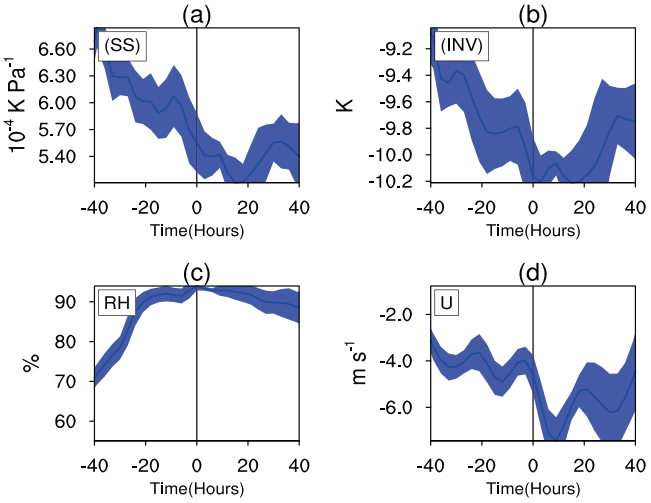

FIGURE 10 The composite time series, averaged over the MTC region (15–20°N, 65–72°E), with 0 h corresponding to the time of maximum intensification, approximately 70 h into the simulation. The panels display (a) the static stability parameter at 800 hPa; (b) $T_{900} - T_{700}$, representing the strength of the inversion (INV); (c) the mean relative humidity, averaged over the 550–650 hPa layer; and (d) the zonal wind, averaged over the 550–650 hPa layer. The shaded blue region represents the width of one standard deviation among ensemble members. [Colour figure can be viewed at wileyonlinelibrary.com]

and humidity exhibit trends that align with the middle troposphere easterlies over western India (Figure 10d). Additionally, the increase in middle troposphere humidity also indicates the contribution of convection to vortex stretching. Essentially, Figures 2,3, and 10 collectively suggest that the middle troposphere easterlies, enhanced by the Bay of Bengal system, alter the thermal profile over the Arabian Sea and western India significantly. This alteration destabilizes the lower troposphere, reduces dry-air mixing from the west and northwest, and facilitates the moistening of the middle troposphere. These conditions provide an optimal environment for deep convection, convergence, and vortex stretching, leading to the genesis of MTCs. These were the precise features observed during the formation of the July 1963 MTC (Miller & Keshavamurty, 1968).

5.2 | Mechanism denial experiment: Initialization with a cold and dry Bay of Bengal

To further substantiate the influence of the Bay of Bengal systems on the formation of Arabian Sea MTCs, we examine a real instance from July 2020. This instance involves a Bay of Bengal LPS preceding the development of an Arabian Sea MTC, categorically identified as a Type 2a member according to Kushwaha *et al.* (2023). The time

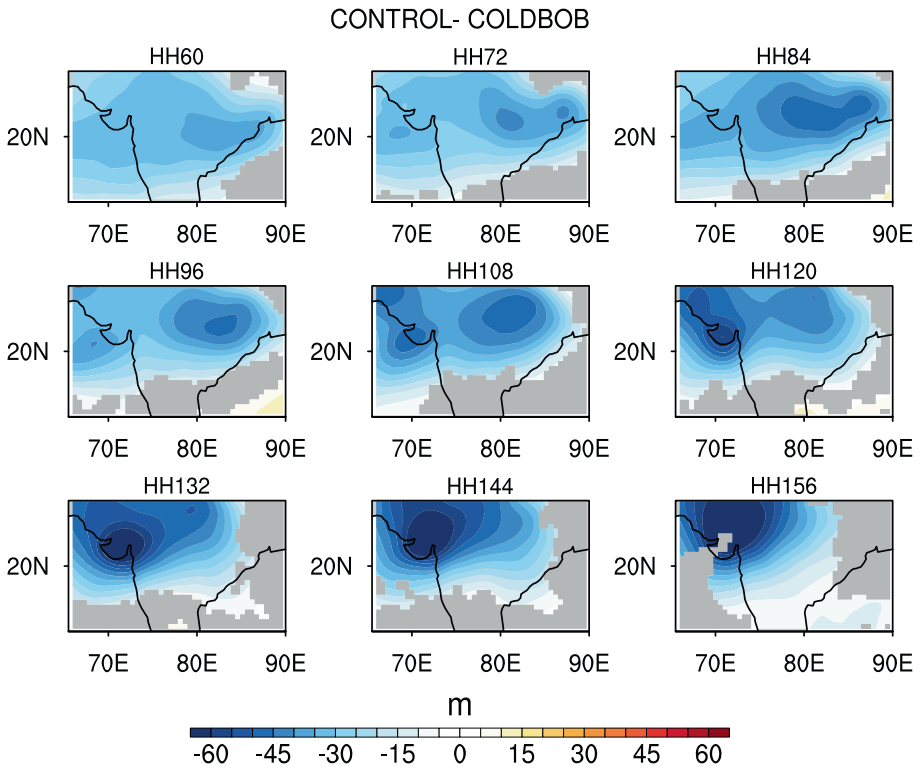

FIGURE 11 Simulated composite ensemble difference in geopotential height at 600 hPa between the control ensemble members and the cold–dry Bay of Bengal case (control–cold and dry Bay of Bengal) for the July 2020 MTC. The ensemble members are initialized on July 1 at 0000, 0600, 1200, and 1800 UTC. The figures depict the simulation results from 60 h (HH60) to 156 h (HH156). Fields are shown only if they differ significantly from zero at a 99% confidence level, as determined by a two-tailed Student's *t*-test; otherwise, the fields are masked. The composite is based on the common UTC dates of all members, with the ensemble member from July 1, 2020, 1800 UTC, serving as the reference. [Colour figure can be viewed at wileyonlinelibrary.com]

evolution of the geopotential height at 600 hPa for four control ensembles, initialized at 0000, 0600, 1200, and 1800 UTC on July 1, 2020, is depicted in Figure S9, spanning from Row 1 to Row 4, respectively. After 72 h of simulation (refer to Figure S9, Column 1), the geopotential height over the Bay of Bengal deepens and a zonal trough emerges over the Arabian Sea and western India. As the Bay of Bengal LPS intensifies further, the trough in the Arabian Sea deepens further between 72 and 120 h. Post 120 h of simulation, an MTC develops within the middle tropospheric trough around 20°N and 72°E in all ensemble members. This MTC intensifies and evolves into an isolated vortex between approximately 120 and 130 h of simulation. Therefore, the model successfully replicates the formation of the July 2020 Type 2a MTC.

We now undertake a mechanism denial experiment to investigate whether an MTC forms in the absence of the Bay of Bengal LPS. The suppression of the Bay of Bengal LPS is achieved by cooling the SST[2] and drying the atmosphere over the Bay of Bengal and East India in the initial conditions, as depicted in Figure S8. With unfavorable conditions prevailing over the Bay of Bengal and East India, the simulated geopotential height at 600 hPa of four ensemble members is depicted in Figure S10. Apart from a slight deepening of height around 96–120 h of model integration, none of the ensemble members exhibits a strong signature of either an LPS in the Bay of Bengal or an MTC over the Arabian Sea. This suggests that, in the absence of the Bay of Bengal LPS, an Arabian Sea system does not form. For further robustness, the composite difference of geopotential height between the control and the cold–dry Bay of Bengal is shown in Figure 11. This clearly indicates that favorable conditions over the Bay of Bengal allow the intensification of Bay of Bengal LPSs, which in turn deepen the trough over the Arabian Sea extending from the Bay of Bengal. These conditions create a favorable environment and support the formation of a MTC over western India and the northeastern Arabian Sea. This implies that with unfavorable conditions over the Bay of Bengal the LPS does not intensify, and consequently the MTC does not form over the Arabian Sea either.

In greater detail, Figure S11 presents the time series of absolute vorticity at 600 hPa, specifically averaged over the Arabian Sea MTCs, for each ensemble member in both the control and cold–dry Bay of Bengal simulations. It is noteworthy that the vorticity in the northeast Arabian Sea consistently remained lower than that in the control run throughout the simulation period. Moreover, the cold–dry Bay of Bengal experiments exhibited a continuous decrease in absolute vorticity. This pattern indicates unfavorable conditions over the Arabian Sea compared with the control run, despite the unfavorable forcing being restricted to the Bay of Bengal. These observations suggest compellingly that the presence of an LPS in the Bay of Bengal, along with its remote effects, plays a crucial role in the distribution of vorticity, horizontal shear, and middle troposphere moisture over the Arabian Sea. Consequently, the frequent co-occurrence of LPSs in the Bay of Bengal

and MTCs over the Arabian Sea cannot be dismissed as coincidental. Rather, it implies that the Bay of Bengal LPSs, with their associated convective heating and remote response, are critical in creating conditions conducive for the formation and, to some extent, the maintenance of Arabian Sea MTCs.

However, it is important to note that, while the majority of in situ Type-2a MTCs are influenced by the Bay of Bengal system, not all MTCs in the Arabian Sea necessarily require the involvement of this system. In fact, Type 2b MTCs, which emerge during the early monsoon season, are generated by the monsoon vortex, and Type 2c MTCs also undergo in situ genesis but originate from precursors in the southern Bay of Bengal (Kushwaha *et al.*, 2023). Notably, Type 2c MTCs, being the weakest category among all MTCs, form under unfavorable conditions over the Bay of Bengal (Kushwaha *et al.*, 2023). This observation underscores the significance of the Bay of Bengal systems, their associated convection, and remote teleconnections in the majority of rainy in situ MTCs in the Arabian Sea.

6 | CONCLUSIONS

A consistent theme observed in previous research, from the seminal work of Miller and Keshavamurty (1968) to more recent studies by Choudhury *et al.* (2018) and the comprehensive objective classification of mid-troposphere cyclones (MTCs) by Kushwaha *et al.* (2023), is the close association between rainy MTCs over western India and the presence of low-pressure systems (LPSs) over the Bay of Bengal. It has been observed that, in many instances, a LPS in the Bay of Bengal precedes the formation of MTCs in the Arabian Sea. Through a systematic set of numerical experiments presented in this study, we have demonstrated that this coexistence is not coincidental; rather, the Bay of Bengal cyclonic systems play a crucial role in the genesis of Arabian Sea MTCs.

We initiated the analysis by examining a composite of MTC genesis events where LPSs in the Bay of Bengal preceded and coexisted with the Arabian Sea MTCs (referred to as Type 2a MTCs in Kushwaha *et al.*, 2023). Conducting a lag composite of dynamical and thermodynamic fields for Type 2a MTCs revealed that the formation and intensification of Bay of Bengal systems accompanied a westward-extending middle troposphere trough. This trough, akin to an off-equatorial heat-induced Gill-type response, extended from the Bay of Bengal to the Arabian Sea. The middle troposphere zonal trough enhanced the horizontal zonal shear over western India and established middle tropospheric easterlies over northwest India. These middle troposphere easterlies prevented the mixing of dry and hot air from the desert regions to the north and west, resulting in a depletion of the low-level inversion layer and destabilization of the lower troposphere. Consequently, moistening of the middle troposphere occurred over the Arabian Sea and western India. Given that this region is typically unfavorable for moist convective activity climatologically, the moistening of the middle troposphere creates favorable conditions for deep convection to occur. These alterations in the dynamic and thermodynamic environment over the Arabian Sea, triggered by the presence of Bay of Bengal systems, provide a fertile ground for the genesis and growth of MTCs

The apparent link between Arabian Sea MTC formation and Bay of Bengal LPSs was further explored with numerical experiments. Two sets of experiments were performed: first, with added "bogus vortices or LPSs" over the Bay of Bengal on top of June–July climatology, and, second, the effect of preventing the formation or weakening of Bay of Bengal LPSs on MTC formation was studied by cooling and drying the Bay of Bengal. Interestingly, in most of the ensemble members where bogus vortices were introduced over specific locations of the Bay of Bengal (where LPSs are most frequently seen before Type 2a MTC formation in observation), the genesis of MTCs took place over the Arabian Sea in 2.5–4 days of model simulations within the induced middle troposphere trough. With the addition of a bogus vortex over the Bay of Bengal, a westward-extending trough formed, stretching from the Bay of Bengal up to the Arabian Sea; as a result, easterlies were established north of the trough axis (around 20°N) and westerlies to the south. This modified flow enhanced the horizontal shear and background vorticity. Middle troposphere easterlies north of the trough prevented dry-air intrusion from the west and north, reduced the low-level inversion, and destabilized the lower troposphere. These features in the numerical simulations agree with the reanalysis-based characterization of the role of Bay of Bengal LPSs in the development of Type 2a MTCs. Furthermore, the vorticity budget of induced MTCs shows that, during the first 24 h of MTC formation, advection of absolute vorticity and tilting accounted for the intensification. However, during the rapid intensification phase, vortex stretching dominated. The β-term remained positive throughout; however, it contributed mainly in the early phase of intensification. Vertical advection was initially quite weak, but it did contribute to the vorticity tendency in the middle troposphere in the later stages of MTC development.

A mechanism denial experiment involving the cooling and drying of the Bay of Bengal was conducted to confirm the link between LPSs in the Bay of Bengal and the genesis of MTCs in the Arabian Sea. The experiment consisted of a control run where an actual Arabian Sea MTC was successfully simulated following the formation

of an LPS over the Bay of Bengal. Subsequently, the Bay of Bengal was artificially cooled and dried to suppress and weaken the formation of Bay of Bengal LPSs. In the control experiment, the LPS over the Bay of Bengal intensified, leading to the development of a westward-extending trough. This resulted in the strengthening of horizontal shear and the establishment of easterly winds. Consequently, an MTC formed over the Arabian Sea as expected. However, in the experiment with the cooled and dried Bay of Bengal, the LPS over the Bay of Bengal failed to intensify. As a result, the westward-extending trough did not develop, and the horizontal shear and easterly winds remained weak. Consequently, an MTC did not form over the Arabian Sea. These findings provide compelling evidence supporting the notion that the coexistence of the Bay of Bengal system during the formation of Arabian Sea MTCs is not a mere coincidence. Instead, the genesis and maintenance of the majority of Type 2a MTCs can be attributed directly to the dynamic influence of LPSs over the Bay of Bengal. The mechanism denial experiment, by dampening the formation of Bay of Bengal LPSs through cooling and drying, clearly demonstrated the crucial role of these systems in the development of MTCs over the Arabian Sea.

It is crucial to acknowledge that these findings, focusing on the impact of a cyclonic system over the Bay of Bengal, pertain specifically to Type 2a MTCs. Nevertheless, MTCs exist that do not require the presence of an LPS over the Bay of Bengal and are triggered by alternate precursors. For instance, Type 2b MTCs evolve from the precursors of the monsoon onset vortex, while Type 2c MTCs emerge from precursors in the southern Bay of Bengal (Kushwaha *et al.*, 2023). Consequently, the outcomes discussed here are particularly relevant to Type 2a in situ MTCs, where the monsoon LPS coexists and precedes over the Bay of Bengal in favorable locations. It is also imperative to recognize that large-scale conditions significantly influence the capacity of LPSs over the Bay of Bengal to initiate MTCs effectively. As Kushwaha *et al.* (2023) elucidates, most Type 2a MTCs develop when the Boreal Summer Intraseasonal Oscillation (BSISO) is in phases 4 and 5. Similarly, BSISO also modulates monsoon LPS formation over the Bay of Bengal (Karmakar *et al.*, 2021), potentially enhancing the background moisture, vorticity, and vertical shear conducive for such interactions. Moreover, LPSs that follow southern trajectories prove more adept at triggering MTCs, possibly owing to their ability to shift the monsoon trough southward and amplify shear over the Arabian Sea.

While the dynamical link between the Bay of Bengal LPS and Arabian Sea MTCs is becoming clear, several areas remain uncharted and warrant comprehensive exploration. The modulation of MTC–LPS events by different phases of the BSISO, for example, is an aspect yet to be fully deciphered. While we hypothesize that heat-induced circulations are integral to this teleconnection, delving into the characteristics and roles of eddy–mean-flow interactions and vertical shear in various phases of the BSISO could shed light on the efficacy of these remote teleconnections. Furthermore, given the proximity of MTC formation to the Western Ghats and the Deccan Plateau's topography in southern India, its influence on these teleconnections merits in-depth study. Investigating these aspects will likely broaden our comprehension of remotely induced cyclones, enhance their predictability, and potentially aid in mitigating the impacts of extreme rainfall events they may cause.

ACKNOWLEDGMENTS

We extend our sincere gratitude to two anonymous reviewers for their constructive guidance, which significantly improved the article. We also acknowledge the European Centre for Medium-Range Weather Forecasts (ECMWF) for providing the ERA-5 reanalysis data, and the National Center for Atmospheric Research/University Corporation for Atmospheric Research (NCAR/UCAR) for making the Weather Research and Forecasting (WRF) open-source code available for our simulations. Additionally, we are grateful to the National Centers for Environmental Prediction (NCEP) for supplying the Final Analysis (FNL) data, essential for initializing our model simulations.

DATA AVAILABILITY STATEMENT

The datasets supporting the conclusions of this study are openly available in the following public repositories. *ERA-5 Reanalysis Data*: This dataset provides a comprehensive reanalysis of global atmospheric conditions and is used for composite analysis. It can be accessed via its DOI link at https://doi.org/10.24381/cds.bd0915c6. *FNL (Final) Operational Global Analysis Data*: Offering high-resolution, global meteorological data, this dataset is used for initializing the WRF model and can be downloaded from https://doi.org/10.5065/D6M043C6. *MTC–LPS Event Data*: Data on various classes of MTC, as described in Kushwaha *et al.* (2023), relevant to this study are available in a GitHub repository, facilitating direct download at https://github.com/pradeepkus/MTC_DATA.git. *Simulation Data*: Detailed data from simulations performed in this study are available upon reasonable request, due to the large data size. Interested researchers may contact the corresponding author to access these data.

ENDNOTES

[1]The locations of the other ensemble members in regions A2–A4 were chosen to assess the sensitivity of MTC induction to varying positions of lows in the Bay of Bengal. The intensity and size of these vortices were set to match IMD data and observed sizes of Bay of

Bengal LPSs (Hunt *et al.*, 2016), respectively. Due to the weaker and smaller nature of these vortices, which are advected by the mean flow and take longer to intensify, these specific values were selected through trial and error.

[2]Note: the SST remains constant throughout the simulations, that is, these are uncoupled simulations.

ORCID

Pradeep Kushwaha https://orcid.org/0000-0002-9403-5217

REFERENCES

Ames, W.F. (2014) *Numerical methods for partial differential equations*. Boston MA: Academic Press.

Arnason, G. (1958) A convergent method for solving the balance equation. *Journal of Atmospheric Sciences*, 15(2), 220–225. Available from: https://doi.org/10.1175/1520-0469(1958)015<0220:ACMFST>2.0.CO;2

Boos, W.R., Hurley, J.V. & Murthy, V.S. (2015a) Adiabatic westward drift of Indian monsoon depressions. *Quarterly Journal of the Royal Meteorological Society*, 141, 1035–1048. Available from: https://doi.org/10.1002/qj.2454

Boos, W.R., Hurley, J.V. & Murthy, V.S. (2015b) Adiabatic westward drift of indian monsoon depressions. *Quarterly Journal of the Royal Meteorological Society*, 141(689), 1035–1048. Available from: https://doi.org/10.1002/qj.2454

Carr, F.H. (1977) Mid-tropospheric cyclones of the summer monsoon. *Pure and Applied Geophysics*, 115(5-6), 1383–1412. Available from: https://doi.org/10.1007/978-3-0348-5759-8.15

Charney, J. (1955) The use of the primitive equations of motion in numerical prediction. *Tellus*, 7(1), 22–26. Available from: https://doi.org/10.1111/j.2153-3490.1955.tb01138.x

Choudhury, A.D., Krishnan, R., Ramarao, M.V.S., Vellore, R., Singh, M. & Mapes, B. (2018) A phenomenological paradigm for midtropospheric cyclogenesis in the Indian summer monsoon. *Journal of the Atmospheric Sciences*, 75(9), 2931–2954. Available from: https://doi.org/10.1175/JAS-D-17-0356.1

Das, S.K., Thatte, T., Uma, K.N., Krishna, U.V.M. & Saha, S.K. (2021) Characteristics of temperature inversion from radiosonde measurements in the western ghats region. *Atmospheric Research*, 250, 105391. Available from: https://doi.org/10.1016/j.atmosres.2020.105391

Davis, C.A., Ahijevych, D.A. & Trier, S.B. (2002) Detection and prediction of warm season midtropospheric vortices by the rapid update cycle. *Monthly Weather Review*, 130(1), 24–42. Available from: https://doi.org/10.1175/1520-0493(2002)130<0024:DAPOWS>2.0.CO;2

Davis, C.A. & Low-Nam, S. (2001) The ncar-afwa tropical cyclone bogussing scheme. *Air Force Weather Agency (AFWA) Rep*, 12 https://www.researchgate.net/publication/255029602_The_NCAR-AFWA_Tropical_Cyclone_Bogussing_Scheme

Diaz, M. & Boos, W.R. (2019a) Barotropic growth of monsoon depressions. *Quarterly Journal of the Royal Meteorological Society*, 145(719), 824–844. Available from: https://doi.org/10.1002/qj.3467

Diaz, M. & Boos, W.R. (2019b) Monsoon depression amplification by moist barotropic instability in a vertically sheared environment. *Quarterly Journal of the Royal Meteorological Society*, 145(723), 2666–2684. Available from: https://doi.org/10.1002/qj.3585

Ding, A., Wang, T., Zhao, M., Wang, T. & Li, Z. (2004) Simulation of sea-land breezes and a discussion of their implications on the transport of air pollution during a multi-day ozone episode in the pearl river delta of china. *Atmospheric Environment*, 38(39), 6737–6750. Available from: https://doi.org/10.1016/j.atmosenv.2004.09.017

Dwivedi, S., Viswanadhapalli Yesubabu, M., Ratnam, V., Dasari, H.P., Sabique Langodan, S.T., Raj, A. et al. (2021) Variability of monsoon inversion over the arabian sea and its impact on rainfall. *International Journal of Climatology*, 41, E2979–E2999. Available from: https://doi.org/10.1002/joc.6896

Francis, P.A. & Gadgil, S. (2006) Intense rainfall events over the west coast of india. *Meteorology and Atmospheric Physics*, 94(1-4), 27–42. Available from: https://doi.org/10.1007/s00703-005-0167-2

Fredrick, S., Davis, C., Gill, D. & Low-Nam, S. (2009) *Bogussing of tropical cyclones in wrf version 3.1*, Vol. 1. NCAR Technical Document P, p. 6.

Gill, A.E. (1980) Some simple solutions for heat-induced tropical circulation. *Quarterly Journal of the Royal Meteorological Society*, 106(449), 447–462. Available from: https://doi.org/10.1002/qj.49710644905

Goswami, B.N., Keshavamurty, R.N. & Satyan, V. (1980) Role of barotropic, baroclinic and combined barotropic-baroclinic instability for the growth of monsoon depressions and mid-tropospheric cyclones. *Proceedings of the Indian Academy of Sciences-Earth and Planetary Sciences*, 89(1), 79–97. Available from: https://doi.org/10.1007/BF02841521

Goswami, B.N. (1987) A mechanism for the west-north-west movement of monsoon depressions. *Nature*, 326(6111), 376–378. Available from: https://doi.org/10.1038/326376a0

Hersbach, H., Bell, B., Berrisford, P., Hirahara, S., Horányi, A., Muñoz-Sabater, J. et al. (2020) The era5 global reanalysis. *Quarterly Journal of the Royal Meteorological Society*, 146(730), 1999–2049. Available from: https://doi.org/10.1002/qj.3803

Holton, J.R. (1973) An introduction to dynamic meteorology. *American Journal of Physics*, 41(5), 752–754. Available from: https://doi.org/10.1119/1.1987371

Hunt, K.M.R., Turner, A.G., Innes, P.M., Parker, D.E. & Levine, R.C. (2016) On the structure and dynamics of Indian monsoon depressions. *Monthly Weather Review*, 144, 3391–3416. Available from: https://doi.org/10.1175/MWR-D-15-0138.1

Jian, G.-J. & Chun-Chieh, W. (2008) A numerical study of the track deflection of supertyphoon haitang (2005) prior to its landfall in Taiwan. *Monthly Weather Review*, 136(2), 598–615. Available from: https://doi.org/10.1175/2007MWR2134.1

Kalnay, E., Kanamitsu, M., Kistler, R., Collins, W., Deaven, D., Gandin, L. et al. (1996) The ncep/ncar 40-year reanalysis project. *Bulletin of the American Meteorological Society*, 77(3), 437–472. Available from: https://doi.org/10.1175/1520-0477(1996)077<0437:TNYRP>2.0.CO;2

Karmakar, N., Boos, W.R. & Misra, V. (2021) Influence of intraseasonal variability on the development of monsoon depressions. *Geophysical Research Letters*, 48(2), e2020GL090425. Available from: https://doi.org/10.1029/2020GL090425

Kesarkar, A.P., Dalvi, M., Kaginalkar, A. & Ojha, A. (2007) Coupling of the weather research and forecasting model with aermod for pollutant dispersion modeling. A case study for pm10 dispersion over Pune, India. *Atmospheric Environment*, 41(9), 1976–1988. Available from: https://doi.org/10.1016/j.atmosenv.2006.10.042

Komaromi, W.A., Majumdar, S.J. & Rappin, E.D. (2011) Diagnosing initial condition sensitivity of typhoon sinlaku (2008) and hurricane ike (2008). *Monthly Weather Review*, 139(10), 3224–3242. Available from: https://doi.org/10.1175/MWR-D-10-05018.1

Krouse, K.D. & Sobel, A.H. (2010) An observational study of multiple tropical cyclone events in the western north pacific. *Tellus A: Dynamic Meteorology and Oceanography*, 62(3), 256–265. Available from: https://doi.org/10.1111/j.1600-0870.2010.00435.x

Krouse, K.D., Sobel, A.H. & Polvani, L.M. (2008) On the wavelength of the rossby waves radiated by tropical cyclones. *Journal of the Atmospheric Sciences*, 65(2), 644–654. Available from: https://doi.org/10.1175/2007JAS2402.1

Kuester, M.A., Alexander, M.J. & Ray, E.A. (2008) A model study of gravity waves over hurricane humberto (2001). *Journal of the Atmospheric Sciences*, 65(10), 3231–3246. Available from: https://doi.org/10.1175/2008JAS2372.1

Kushwaha, P., Sukhatme, J. & Nanjundiah, R. (2021) A global tropical survey of midtropospheric cyclones. *Monthly Weather Review*, 149(8), 2737–2753. Available from: https://doi.org/10.1175/MWR-D-20-0222.1

Kushwaha, P., Sukhatme, J. & Nanjundiah, R.S. (2023) Classification of mid-tropopsheric cyclones over the Arabian sea and western India. *Quarterly Journal of the Royal Meteorological Society*, 149(754), 1572–1592. Available from: https://doi.org/10.1002/qj.4466

Lo, J.C.-F., Yang, Z.-L. & Pielke Sr, R.A. (2008) Assessment of three dynamical climate downscaling methods using the weather research and forecasting (wrf) model. *Journal of Geophysical Research: Atmospheres*, 113(D9). Available from: https://doi.org/10.1029/2007JD009216

Low-Nam, S. & Davis, C. (2001) Development of a tropical cyclone bogussing scheme for the mm5 system. In Preprints, 11th PSU–NCAR mesoscale model users' workshop, Boulder, CO, PSU–NCAR, volume 130, page 134.

Mak, M., & Jim Kao, C.-Y. (1982) An instability study of the onset-vortex of the southwest monsoon, 1979. *Tellus*, 34(4), 358–368. Available from: https://onlinelibrary.wiley.com/doi/pdf/10.1111/j.2153-3490.1982.tb01825.x

Mak, M.-K. (1975) The monsoonal mid-tropospheric cyclogenesis. *Journal of the Atmospheric Sciences*, 32(12), 2246–2253. Available from: https://doi.org/10.1175/1520-0469(1975)032<2246:TMMTC>2.0.CO;2

Mapes, B. (2011) Heaviest precipitation events, 1998-2007: a near-global survey. In: *The global monsoon system: research and forecast*. World Scientific, pp. 15–22. Available from: https://doi.org/10.1142/9789814343411.0002

Masunaga, H. (2014) Free-tropospheric moisture convergence and tropical convective regimes. *Geophysical Research Letters*, 41(23), 8611–8618.

Melhauser, C. & Zhang, F. (2012) Practical and intrinsic predictability of severe and convective weather at the mesoscales. *Journal of the Atmospheric Sciences*, 69(11), 3350–3371.

Miller, F.R. & Keshavamurty, R.N. (1968) Structure of an Arabian Sea summer monsoon system. International Indian Ocean Experiment, Metero. Monog, 1.

Muraleedharan, P.M., Mohankumar, K. & Sivakumar, K.U. (2013) A study on the characteristics of temperature inversions in active and break phases of indian summer monsoon. *Journal of Atmospheric and Solar-Terrestrial Physics*, 93, 11–20. Available from: https://doi.org/10.1016/j.jastp.2012.11.006

Murthy, V.S. & Boos, W.R. (2019) Understanding the vertical structure of potential vorticity in tropical depressions. *Quarterly Journal of the Royal Meteorological Society*, 145(722), 1968–1991. Available from: https://doi.org/10.1002/qj.3539

Narayanan, M.S., Rao, B.M., Shah, S., Prasad, V.S. & Bhat, G.S. (2004) Role of atmospheric stability over the Arabian sea and the unprecedented failure of monsoon 2002. *Current Science*, 86(7), 938–947. https://www.jstor.org/stable/24109276

Peckham, S.E., Smirnova, T.G., Benjamin, S.G., Brown, J.M. & Kenyon, J.S. (2016) Implementation of a digital filter initialization in the wrf model and its application in the rapid refresh. *Monthly Weather Review*, 144(1), 99–106. Available from: https://doi.org/10.1175/MWR-D-15-0219.1.

Ramage, C.S. (1964) *Some preliminary research results from the international meteorological centre*. New Zealand: Proc. WMO Symposium on Tropical Meteorology, pp. 403–408.

Raymond, D.J., López Carrillo, C. (2011) The vorticity budget of developing typhoon nuri (2008). *Atmospheric Chemistry and Physics*, 11(1), 147–163. Available from: https://doi.org/10.5194/acp-11-147-2011

Raymond, D., Fuchs, Ž., Gjorgjievska, S. & Sessions, S. (2015) Balanced dynamics and convection in the tropical troposphere. *Journal of Advances in Modeling Earth Systems*, 7(3), 1093–1116. Available from: https://doi.org/10.1002/2015MS000467

Russell, J.O.H. & Aiyyer, A. (2020) The potential vorticity structure and dynamics of african easterly waves. *Journal of the Atmospheric Sciences*, 77(3), 871–890. Available from: https://doi.org/10.1175/JAS-D-19-0019.1

Saikranthi, K., Radhakrishna, B., Rao, T.N. & Satheesh, S.K. (2019a) Variability in vertical structure of precipitation with sea surface temperature over the Arabian sea and the bay of Bengal as inferred by tropical rainfall measuring mission precipitation radar measurements. *Atmospheric Chemistry and Physics*, 19(15), 10423–10432. Available from: https://doi.org/10.5194/acp-19-10423-2019

Saikranthi, K., Radhakrishna, B., Thota, N.R. & Satheesh, S.K. (2019b) Differences in the association of sea surface temperature—precipitating systems over the bay of Bengal and the Arabian sea during southwest monsoon season. *International Journal of Climatology*, 39(11), 4305–4312. Available from: https://doi.org/10.1002/joc.6074

Schenkel, B.A. (2016) A climatology of multiple tropical cyclone events. *Journal of Climate*, 29(13), 4861–4883. Available from: https://doi.org/10.1175/JCLI-D-15-0048.1

Schenkel, B.A. (2017) Are multiple tropical cyclone events similar among basins? *Journal of Climate*, 30(15), 5805–5813. Available from: https://doi.org/10.1175/JCLI-D-17-0088.1

Someshwar Das, R., Ashrit, M.W., Moncrieff, M.D., Gupta, J.D., Liu, C. & Kalsi, S.R. (2007) Simulation of intense organized convective precipitation observed during the Arabian sea monsoon experiment (armex). *Journal of Geophysical Research: Atmospheres*, 112(D20). Available from: https://doi.org/10.1029/2006JD007627

Van Nguyen, H. & Chen, Y.-L. (2011) High-resolution initialization and simulations of typhoon morakot (2009). *Monthly Weather Review*, 139(5), 1463–1491. Available from: https://doi.org/10.1175/2011MWR3505.1

Wang, D., Liang, X., Zhao, Y. & Wang, B. (2008) A comparison of two tropical cyclone bogussing schemes. *Weather and Forecasting*, 23(1), 194–204. Available from: https://doi.org/10.1175/2007WAF2006094.1

Xie, S.-P., Xu, H., Saji, N.H., Wang, Y. & Liu, W.T. (2006) Role of narrow mountains in large-scale organization of Asian monsoon convection. *Journal of Climate*, 19(14), 3420–3429. Available from: https://doi.org/10.1175/JCLI3777.1

Yang, M.-J., Zhang, D.-L. & Huang, H.-L. (2008) A modeling study of typhoon nari (2001) at landfall. Part i: topographic effects. *Journal of the Atmospheric Sciences*, 65(10), 3095–3115. Available from: https://doi.org/10.1175/2008JAS2453.1

Zhang, C., Wang, Y. & Hamilton, K. (2011) Improved representation of boundary layer clouds over the southeast pacific in arw-wrf using a modified tiedtke cumulus parameterization scheme. *Monthly Weather Review*, 139(11), 3489–3513. Available from: https://doi.org/10.1175/2008JAS2453.1

SUPPORTING INFORMATION

Additional supporting information can be found online in the Supporting Information section at the end of this article.

How to cite this article: Kushwaha, P., Sukhatme, J. & Nanjundiah, R.S. (2024) Role of Bay of Bengal low-pressure systems in the formation of mid-tropospheric cyclones over the Arabian Sea and western India. *Quarterly Journal of the Royal Meteorological Society*, 1–21. Available from: https://doi.org/10.1002/qj.4726

APPENDIX A. TROPICAL CYCLONE BOGUS VORTEX SCHEME IN WRF

A.1 Vortex addition scheme

As in Davis *et al.* (2002), the process of construction of a bogus vortex method in WRF is based on the following assumptions.

1. The vortex is assumed to be axis-symmetric.
2. The mass and momentum fields are assumed to be in nonlinear balance.
3. Radius of maximum wind is specified.
4. The core of the system is assumed to be near-saturated.
5. Maximum winds of bogus storms are a predetermined fraction of maximum observed winds.

The user-specified vortex wind profile is given by the simple Rankine vortex, namely,

$$v = A(z)F(r), \tag{A1}$$

where

$$F(r) = \frac{v_m}{r_m} r \; ; (r \le r_m) \quad \text{and} \quad F(r) = \frac{v_m}{r_m^{\alpha}} r^{\alpha} \; ; (r > r_m). \tag{A2}$$

Here v_m is the maximum wind at a radius of maximum wind, r_m, and $\alpha = -0.75$ is the empirical constant used to reduce the mismatch between the vortex winds and the influence of other systems at large radii. Vortex wind amplitude and height dependence is defined by $A(z)$. The assumption is that the maximum azimuthally averaged wind is $0.75V$, where V is the user-defined maximum wind. The vertical weighting function, $A(z)$, is 1 up to 600 hPa and decreases linearly to 150 hPa and above. Within the radius of maximum wind, the relative humidity is assumed to be nearly saturated. Outside twice the radius of maximum wind, climatological humidity is prescribed, and, between the two, radii humidity is linearly relaxed from saturation to climatology. Once the vortex winds are defined, the stream function is known. Then the equation of nonlinear balance (Equation A3), which relates the stream function and geopotential height fields, is used to calculate the geopotential height perturbation (Charney, 1955):

$$\nabla^2\psi + \nabla\psi.\nabla f - \frac{2}{f}\left[\left(\frac{\partial^2\psi}{\partial x \partial y}\right)^2 - \frac{\partial^2\psi}{\partial x^2}\frac{\partial^2\psi}{\partial y^2}\right] = \frac{\nabla^2\phi}{f}. \tag{A3}$$

In Equation (A3), ψ represents the stream function, ϕ represents the geopotential height, and f is Coriolis parameter. The above Poisson equation can be solved numerically, provided that the appropriate solution strategy is used to ensure convergence (Ames, 2014; Arnason, 1958). Finally, once the geopotential height perturbations are known, they are used to calculate the temperature perturbations by hydrostatic balance:

$$\left(\frac{\partial\phi}{\partial(d\ln p)} = -RT\right).$$

A.2 Vortex removal scheme

The initial stage of the vortex removal process requires precise identification of the storm-associated vortex within the preliminary guess field. The preferred approach for vortex elimination in WRF as listed in Davis *et al.* (2002) involves modifying the vorticity, geostrophic vorticity, and divergence, followed by computation of the non-divergent stream function, geopotential, and velocity potential changes, leading to a revised velocity field.

The relationship between non-divergent winds, stream function, and vorticity is

$$\nabla^2\psi = \zeta, \tag{A4}$$

$$\mathbf{v}_\psi = \hat{k} \times \nabla\psi, \tag{A5}$$

where ψ is the stream function for non-divergent wind, ζ is relative vorticity, and $\mathbf{v}_\psi$ is the non-divergent wind.

The non-divergent wind associated with the initial storm is defined by setting vorticity to zero outside r_m and specifying $\psi = 0$ on the lateral boundaries of the domain, solving Equation (A4) for a perturbation stream function ψ' on all pressure surfaces, and calculating $\mathbf{v}'_\psi$ using Equation (A5), which can then be subtracted from the first-guess wind fields.

To remove divergent wind and pressure anomalies, Equations (A6) and (A7) can be used. These are the same as (A4) and (A5), except that they involve the use of divergence and geopotential height anomalies. The equations for removing divergent winds are

$$\nabla^2 \chi = \delta, \tag{A6}$$

$$\mathbf{v}_\chi = \nabla \chi, \tag{A7}$$

where χ and δ represent the velocity potential and divergence, respectively.

To remove the geopotential height anomalies, we use

$$\nabla^2 \phi = \zeta_g f_0, \tag{A8}$$

$$\mathbf{v}_g = \hat{k} \times \nabla \phi, \tag{A9}$$

where ϕ is the geopotential anomaly, ζ_g the geostrophic vorticity, and f_0 the Coriolis parameter at the storm center. The above equations can be solved by setting geostrophic vorticity $\zeta_g = 0$ outside $r = r_m$ and solving for ϕ', which then can be subtracted from the initial guess.

The removal of the temperature anomaly field related to the first-guess fields can be performed using the hydrostatic relation

$$\frac{\partial \phi'}{\partial \ln(p)} = -RT, \tag{A10}$$

where R is the gas constant and p the pressure. This step ensures the initial field retains only background wind and temperature at the original storm location. Although the current method does not modify the background flow, it allows for identifying and correcting deviations between the background steering flow and the storm track.

APPENDIX B

In the second set of experiments, the Bay of Bengal (BOB) sea-surface temperature was cooled by adding a Gaussian temperature perturbation of the following form:

$$S(x,y) = S_0 \exp\left[\left(\frac{(x-x_0)^2}{2\sigma_x^2}\right) + \left(\frac{(y-y_0)^2}{2\sigma_y^2}\right)\right], \tag{B1}$$

where S is the SST perturbation, x_0 and y_0 are the longitude and latitude of the center of the SST blob, S_0 (=280 K) is the SST value at the center of the blob, and σ_x and σ_y determine the smoothness and extent of the blob.